ELSEVIER

Title

D. Siedel, T. Helfer, J. Besson, O. Fandeur, N. Pignet

Abstract

The Hybrid High Order (HHO) method is a powerful discretization method which has only been recently applied to non linear computational mechanics.

The Hybrid High Order method divides the domain of interest in cells of arbitrary polyhedral shape, whose boundaries form the skeleton of the mesh, and introduces two kinds of degrees of freedom: the displacements in cells and the displacements of the skeleton.

Most introductory materials to the HHO method is focused on mathematical aspects. While they are important, an approach based on physical considerations would help spreading this method to the computational mechanics and engineering communities.

This paper derives Hybrid High Order method from the classical Hu–Washizu functional.

Practical implementation of the method is discussed in depth using notations closed to the ones used in standard finite elements textbooks, highlighting the use of polyhedral cells and the use of approximation spaces based on polynomials of arbitrary orders.

From the point of view of numerical performances, the elimination of the cell degrees of freedom is mandatory to reduce the size of the stiffness matrix. The standard static condensation, is presented, as well as a novel strategy called "cell equilibrium". Advantages and disadvantages of both strategies are discussed.

The resolution of axi-symmetrical problems, which has seldom, if ever, been discussed in the literature, is then presented.

Numerical examples prove the robustness of the method with regards to volumetric locking

Contents

1. Introduction

The Hybird High Order method (HHO) is a discontinuous discretization method, that takes root in the Discontinuous Galerkin method (DG). From the physical standpoint, DG methods ensure the continuity of the flux across interfaces, by seeking the solution element-wise, hence allowing jumps of the potential across elements. They can be seen as a generalization of Finite Volume methods, and are able to capture physically relevant discontinuities without producing spurious oscillations. The origin of DG methods dates back to the pioneering work of [1], where an hyperbolic formualtion is used to solve the neutron transport equation. The first application of the method to elliptic problems originates in [2] where Nitsche's method [3] is used to weakly impose continuity of the flux across interfaces. In 2002, Hansbo and Larson [4] were the first to consider the Nitsche's classical DG method for nearly incompressible elasticity. They showed, theoretically and numerically, that this method is free from volumetric locking. However, the bilinear form arising from this formulation is not symmetric. A so called interior penalty term has been introduced in [5], leading to the Symmetric Interior Penalty (SIP) DG method. A first study of the method to linear elasticity has been devised by [6], where optimal error estimate has been proved. [7] generalized the Symmetric Interior Penalty method to linear elasticity. In about the same period of time, DG methods were proposed for other linear problems in solid mechanics, such as Timoshenko beams [8], Bernoulli-Euler beam and the Poisson-Kirchhoff plate [9, 10] and Reissner-Mindlin plates [11]. In the mid 2000's, the first applications of DG methods to nonlinear elasticity problems was undertaken by [12, 13], and in 2007, Ortner and Süli [14] carried out the a priori error analysis of DG methods

for nonlinear elasticity. DG methods then sollicitated a vigourus interest, mostly in fluid dynamics [15, 16] due to their local conservative property and stability in convection domniated problems. However, except some applications for instance in fracture mechanics using XFEM methods [17, 18], or gradient plasticity [19, 20] DG methods did not break through in computational solid mechanics because of their numerical cost, since nodal unknowns need be duplicated to define local basis functions in each element. To adress this problem, in the early 2010's, [21, 22] introduced additional faces unknowns on element interfaces for linear elastic problem, hence leading to the hybridization of DG methods, or Hybridizable Discontinuous Galerkin method (HDG). By adding supplementary boundary unknowns, the authors actually allowed to eliminate original cell unknowns by a static condensation process, in order to express the global problem on faces ones only. Extension of HDG methods to non-linear elasticity were first undertaken in [23] and have then fueled intense reaserch works for various applications such as linear and non-linear convection-diffusion problems [24, 25, 26], incompressible stokes flows [26, 27] and non-linear mechanics [28]. In [29, 30], the authors introduced a higher order potential reconstruction operator in the classical HDG formulation for elliptic problems, providing a $h^{k+1}H^1$-norm convergence rate as compared to the ususal h^k-rate. This higher order term coined the name for the so called HHO method. Recent developments of HHO methods in computational mechanics include the incompressible Stokes equations (with possibly large irrotational forces) [31], the incompressible Navier–Stokes equations [32], Biot's consolidation problem [33], and nonlinear elasticity with small deformations [34]

2. The model problem

2.1. The standard Hu–Washizu Lagrangian

This paragraph introduces the standard Hu–Washizu three field principle. For the sake of simplicity, and without loss of generality, let consider the case of an hyperelastic material. Extensions to mechanical behaviours with internal state variables are treated in classical textbooks of computational mechanics. We will treat this extension in the Section 5 discussing the numerical implementation of the Hybrid High Order method and in Section 6 which provides several examples in plasticity.

2.1.1. Description of the mechanical problem and notations

Solid body. Let us consider a solid body whose reference configuration is denoted Ω. At a given time $t > 0$, the body is in the current configuration Ω_t.

Mechanical loading. The body is assumed to be submitted to a body force $\boldsymbol{f}_v$ acting in Ω_t, a prescribed displacement $\boldsymbol{u}_d$ on the Dirichlet boundary $\partial_d\Omega_t$, and a contact load $\boldsymbol{t}_n$ on the Neumann boundary $\partial_n\Omega_t$.

Deformation. The transformation mapping $\boldsymbol{\Phi}$ takes a point from the reference configuration Ω to the current configuration Ω_t such that

$$\boldsymbol{\Phi}\left(X\right) = \boldsymbol{x} = X + \boldsymbol{u}\left(X\right) \tag{1}$$

where X, $\boldsymbol{x}$ and $\boldsymbol{u}$ denote respectively the position in the reference configuration Ω, the position in the current configuration Ω_t and the displacement.

Deformation gradient, gradient of the displacement. The deformation gradient $\underset{\sim}{\boldsymbol{F}}$ is defined as

$$\underset{\sim}{\boldsymbol{F}} = \nabla\boldsymbol{\Phi} = \underset{\sim}{\boldsymbol{I}} + \underset{\sim}{\boldsymbol{G}} \tag{2}$$

where ∇ is the gradient operator in the reference configuration and

$$\underset{\sim}{\boldsymbol{G}} = \nabla\boldsymbol{u} \tag{3}$$

denotes the gradient of the displacement.

Stress tensor. The body is assumed made of an hyperelastic material described by a free energy ψ_Ω which relates the deformation gradient $\underset{\sim}{\boldsymbol{F}}$ and the first Piola-Kirchhoff stress tensor $\underset{\sim}{\boldsymbol{P}}$ such that

$$\underset{\sim}{\boldsymbol{P}} = \frac{\partial\psi_\Omega}{\partial\underset{\sim}{\boldsymbol{F}}} \tag{4}$$

2.1.2. Primal problem and Principle of Virtual Work

Total lagrangian. The total Lagrangian L_Ω^{VW} of the body is defined as the stored energy minus the work of external loadings, as follows:

$$L_\Omega^{VW} = \int_\Omega \psi_\Omega(\underset{\sim}{F}(u)) - \int_\Omega f_V \cdot u - \int_{\partial_N\Omega} t_N \cdot u|_{\partial_N\Omega} \tag{5}$$

where the body forces f_V and conctat tractions t_N in the reference configuration have been obtained from their counterparts f_v and t_n using the Nanson formulae.

Principle of Virtual Works. The displacement u satisfying the mechanical equilibrium minimizes the Lagragian L_Ω^{VW}. The first order variation of Lagrangian is given by:

$$\frac{\partial L_\Omega^{VW}}{\partial u} \cdot \delta u = \int_\Omega \underset{\sim}{P} : \nabla \delta u - \int_\Omega f_V \cdot \delta u - \int_{\partial_N\Omega} t_N \cdot \delta u|_{\partial_N\Omega} \tag{6}$$

which must be null for the the solution displacement. The solution displacement thus satisfies the principle of virtual work:

$$\int_\Omega \underset{\sim}{P} : \nabla \delta u = \int_\Omega f_V \cdot \delta u + \int_{\partial_N\Omega} t_N \cdot \delta u|_{\partial_N\Omega} \quad \forall \delta u$$

2.1.3. The Hu-Washizu Lagrangian

The Hu-Washizu Lagrangian L_Ω^{HW} [35, 36] generalizes the previous variational principle by considering that the gradient of the displacement $\underset{\sim}{G}$ and the first Piola-Kirchoff $\underset{\sim}{P}$ stress are independent unknowns of the problem, such that:

$$L^{HW} = \int_\Omega \psi_\Omega(\underset{\sim}{I} + \underset{\sim}{G}) + (\nabla u - \underset{\sim}{G}) : \underset{\sim}{P} - \int_\Omega f_V \cdot u - \int_{\partial_N\Omega} t_N \cdot u|_{\partial_N\Omega} \tag{7}$$

The solution $(u, \underset{\sim}{G}, \underset{\sim}{P})$ satisfying the mechanical equilibrium minimizes the Lagragian L_Ω^{HW}. The first order variation of the Hu-Washizu Lagragian with respect to $u, \underset{\sim}{G}$, and $\underset{\sim}{P}$ yields

$$\frac{\partial L_\Omega^{HW}}{\partial u} \cdot \delta u = \int_\Omega \underset{\sim}{P} : \nabla \delta u - \int_\Omega f_V \cdot \delta u - \int_{\partial_N\Omega} t_N \cdot \delta u|_{\partial_N\Omega} \qquad \forall \delta u \tag{8a}$$

$$\frac{\partial L_\Omega^{HW}}{\partial \underset{\sim}{P}} : \delta \underset{\sim}{P} = \int_\Omega (\nabla u - \underset{\sim}{G}) : \delta \underset{\sim}{P} \qquad \forall \delta \underset{\sim}{P} \tag{8b}$$

$$\frac{\partial L_\Omega^{HW}}{\partial \underset{\sim}{G}} : \delta \underset{\sim}{G} = \int_\Omega (\frac{\partial \psi}{\partial \underset{\sim}{G}} - \underset{\sim}{P}) : \delta \underset{\sim}{G} \qquad \forall \delta \underset{\sim}{G} \tag{8c}$$

where equation (8b) and (8c) account for (3) and (4) respectively in a weak sense.

2.2. On the use of the Hu-Washizu Lagrangian in mechanics to circumvent volumetric locking

In the continuous framework, the Hu-Washizu functional is not relevant, since equations (8b) and (8c) would hold true in a strong sense.

Pressure swelling formulations. Since volumetric locking is pressure dependent phenomenon, considering for instance a decomposition of the stress and strain fields into *e.g.* devatoric and spherical components, one can express a mixed problem in terms of pressure and swelling, which is at the origin of so-called UPG methods [37, 38, 39]. The scalar pressure and swelling unknowns replace respectively the stress and strain tensorial unknowns in (7) and a modified deformation gradient is introduced in the constitutive equation.

Enhanced assumed strains formulations. Another approach of the use of the Hu-Washizu consists in studying the equilibrium of a single element. Such a framework falls into the scope of so-called Enhanced Assumed Strains methods [40, 41], which results for instance in the B-bar method, that consists in defining a modified derivation operator, such that one gets rid of the three-field formulation, to express the problem in terms of primal unknowns only.

Towards Discontinuous methods. In the present document, we propose an introduction to so-called *non-conformal* methods, by means of the Hu–Washizu Lagrangian. At the origin of these methods is the Discontinuous Galerkin (DG) method, which postulates the discontinuity of the displacement across elements. This feature allows the method to be robust to volumetric locking. However, its formulation takes root in a possibly dry mathematical background, and the ingredients of the method are not introduced in the literature through physical arguments. The goal of the next section aims at introducing the whole framework of non-conformal methods, including the displacement discontinuity, through the Hu–Washizu Lagragian.

3. Introduction to discontinuous methods through a Hu-Washizu formulation

In this section let T a subpart of the body Ω. In the following, one assumes that the cell T is located inside the body Ω, such that its boundary ∂T bears contact loads only. This subpart is in equilibrium with the rest of the body $\Omega \backslash T$ if the displacements and the normal traction are continuous at the boundary ∂T.

Conformal methods. Enforcing the displacement continuity at the interface leads to so-called conformal methods, to which the standard Finite Element (FE), or Lagrange method belongs (see Figure 1(a)).

Discontinuous Galerkin methods. On the contrary, this condition can be weakened by introducing an elastic interface of negligible size between T and $\Omega \backslash T$. This representation is at the basis of Discontinuous Galerkin methods (see Figure 1(b)).

Hybird Discontinuous Galerkin methods. In this paper, we consider hybrid discontinuous Galerkin (HDG) methods, where two elastic interfaces are introduced: one between T and its boundary ∂T and a second one between $\Omega \backslash T$ and ∂T (see Figure 1(c)). Following this idea, we show in this section how the use of the Hu-Hashizu Lagrangian allows to recover the main ingredients of the HDG/HHO methods, namely the *reconstructed gradient* and the *stabilisation operator*.

3.1. Element description

Element geometry. In the following, the cell T is assumed to be convex. It is split into a core part $K \subset T$ with boundary ∂K, and into an interface part $I \subset T$ with boundary $\partial I = \partial K \cup \partial T$, as shown in Figure 1. The interface I has some thickness $\ell > 0$ that is supposed to be small compared to h_T the diameter of T. From a geometrical standpoint, the core par of the element K is an homothety of T by some ratio inferior to 1.

Element boundary description. The boundary ∂T of T is the composition of a Neumann boundary $\partial_N T$ and a Dirichlet $\partial_D T$, if the element T shares a boundary with $\partial_D \Omega$. In the following, for the sake of simplicity, we assume that the element is located inside the body Ω, such that is only subjected to imposed traction forces on $\partial_N T = \partial T$ with $\partial_D T = \emptyset$.
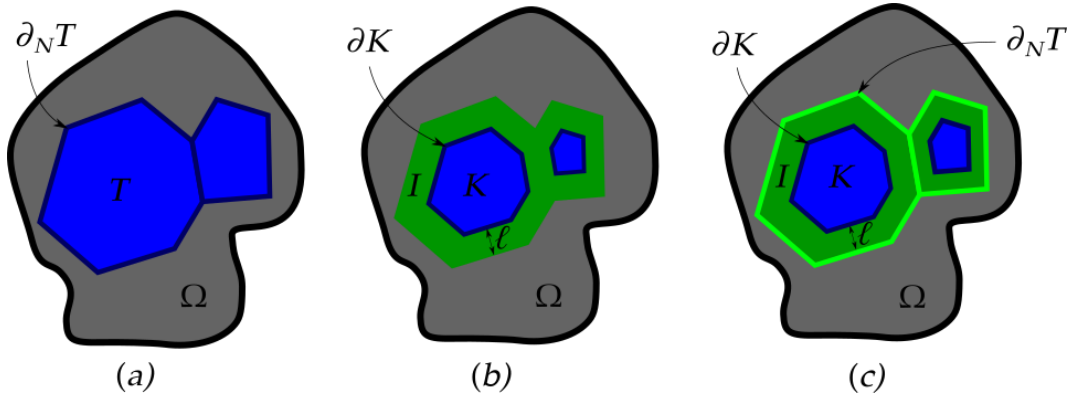
Figure 1. schematic representation of a cell and its surrounding depending on the continuity requirement of the displacement field

Element behaviour. The core of the element K is made out of the same material that composes Ω and behaves according to the free energy potential ψ_Ω. The interface I is made out of a pseudo linear elastic material of Young modulus $\beta(\ell/h_T)$ with a zero Poisson ratio and its behavior is defined by the free energy potential ψ_I such that

$$\psi_I = \frac{1}{2}\beta\frac{\ell}{h_T}\nabla\boldsymbol{u}_I : \nabla\boldsymbol{u}_I \tag{9}$$

where the dimensionless ratio ℓ/h_T balances the accumulated energy with the size of the domain T.

Element loading. The core K is subjected to the volumetric loading $\boldsymbol{f}_V$, and to the traction force applied by the interface I onto ∂K. By continuity, K applies the opposite traction force on I through ∂K. The interface I is also subjected to the exterior traction force $\boldsymbol{t}_{\partial_N T}$ acting on $\partial_N T$, that accounts for the action of the rest of the solid Ω onto the boundary ∂T.

Discplacement, displacement gradient and stress fields. Let note $\boldsymbol{u}_K$ the displacement field, $\underset{\sim}{\boldsymbol{G}}_K$ the displacement gradient field and $\underset{\sim}{\boldsymbol{P}}_K$ the stress field in K. Similarly, let $\boldsymbol{u}_I$ the displacement field, $\underset{\sim}{\boldsymbol{G}}_I$ the displacement gradient field and $\underset{\sim}{\boldsymbol{P}}_I$ the stress field in I. The displacement of the boundary ∂T is denoted $\boldsymbol{u}_{\partial T}$. By continuity of the displacement field between K and ∂T, the displacement $\boldsymbol{u}_I$ verifies

$$\boldsymbol{u}_I|_{\partial K} = \boldsymbol{u}_K|_{\partial K} \tag{10a}$$

$$\boldsymbol{u}_I|_{\partial T} = \boldsymbol{u}_{\partial T} \tag{10b}$$

Hu-Washizu Lagrangian of the element. By combining both the Lagragian of the core K and that of the interface I, one obtains the total Lagragian L_T^{HW} over the element such that

$$L_T^{HW} = \int_K \psi_\Omega + (\nabla\boldsymbol{u}_K - \underset{\sim}{\boldsymbol{G}}_K) : \underset{\sim}{\boldsymbol{P}}_K + \int_I \psi_I + (\nabla\boldsymbol{u}_I - \underset{\sim}{\boldsymbol{G}}_I) : \underset{\sim}{\boldsymbol{P}}_I - \int_K \boldsymbol{f}_V \cdot \boldsymbol{u}_K - \int_{\partial_N T} \boldsymbol{t}_{\partial_N T} \cdot \boldsymbol{u}_{\partial T} \tag{11}$$

3.2. Hypotheses

Since the interface is of negligible volume compared to that of the core, let make the following assumptions on the displacement and the stress fields in the interface.

Displacement in the interface. The displacement in the interface I is assumed to be linear with respect to $\boldsymbol{n}$, such that its gradient is homogeneous in I along $\boldsymbol{n}$

$$\nabla\boldsymbol{u}_I = \frac{\boldsymbol{u}_{\partial T} - \boldsymbol{u}_K|_{\partial K}}{\ell} \otimes \boldsymbol{n} \tag{12}$$

That is, the displacement of the interface I linearly bridges that of the boundary ∂T to that of the bulk K.

Stress in the interface. Furthermore, let assume that $\underset{\sim}{P}_I$ is constant along the direction $\boldsymbol{n}$ in I. By continuity of the traction force across ∂K, the following equality holds true

$$(\underset{\sim}{P}_I|_{\partial K} - \underset{\sim}{P}_K|_{\partial K}) \cdot \boldsymbol{n} = 0 \tag{13}$$

3.3. Towards Hybrid discontinuous methods from the Hu-Washizu Lagrangian

Using the hypotheses stated in Section 3.2 on the displacement field and the stress field in I, one can write (11) as a term depending on the thickness of the interface ℓ and on the core and boundary unknowns only. The reader can refer to Appendix A.1 for more details.

Simplified Hu–Washizu Lagrangian for a vanishing interface. In particular, making the thickness of the interface $\ell \to 0$, such that I vanishes and the core part K identifies to T, one obtains the simplified Hu–Washizu Lagrangian

$$
\begin{aligned}
L_T^{HW} = & \int_T \psi_\Omega + (\nabla \boldsymbol{u}_T - \underset{\sim}{G}_T) : \underset{\sim}{P}_T + \int_{\partial T} (\boldsymbol{u}_{\partial T} - \boldsymbol{u}_T|_{\partial T}) \cdot \underset{\sim}{P}_T|_{\partial T} \cdot \boldsymbol{n} + \int_{\partial T} \frac{\beta}{2h_T} \|\boldsymbol{u}_{\partial T} - \boldsymbol{u}_T|_{\partial T}\|^2 \\
& - \int_T \boldsymbol{f}_V \cdot \boldsymbol{u}_T - \int_{\partial_N T} \boldsymbol{t}_{\partial_N T} \cdot \boldsymbol{u}_{\partial T}
\end{aligned}
\tag{14}
$$

which fully defines the equilibrium of an element for discontinuous methods.

Hybridization of the primal unknown; the HDG and HHO methods. Since the interface I has vanished by making $\ell \to 0$, both $\boldsymbol{u}_T|_{\partial T}$ the trace of the displacement of the core part T onto ∂T and the displacement of the boundary $\boldsymbol{u}_{\partial T}$ coexist on ∂T. The displacement of the element T is thus said to be *hybrid*, and is denoted by the pair $(\boldsymbol{u}_T, \boldsymbol{u}_{\partial T})$.

The special case of DG methods. Replacing $\boldsymbol{u}_{\partial T}$ by $\boldsymbol{u}_{T'}|_{\partial T}$ for any neighboring cell T' amounts to describe the framework of Discontinuous Galerkin methods, where only the core unknown $\boldsymbol{u}_T$ is considered, and the displacement jump on ∂T depends on $\boldsymbol{u}_{T'}|_{\partial T}$ the trace of the displacement of neighboring cells instead.

Conformal Galerkin formulation. By strongly enforcing continuity of the displacement across ∂T such that $\boldsymbol{u}_T|_{\partial T} = \boldsymbol{u}_{\partial T}$, one recovers the Principle of Virtual Work (7), which defines the framework of conformal methods.

Mixed problem for HDG mehtods. By derivation of the total Lagrangian (14) with respect to each variable of the problem, one obtains the weak equations

$$\frac{\partial L_T^{HW}}{\partial \boldsymbol{u}_T} \delta \boldsymbol{u}_T = \int_T \underset{\sim}{P}_T : \nabla \delta \boldsymbol{u}_T - \int_T \boldsymbol{f}_V \cdot \delta \boldsymbol{u}_T - \int_{\partial T} \boldsymbol{\theta}_{\partial T} \cdot \delta \boldsymbol{u}_T|_{\partial T} \qquad \forall \delta \boldsymbol{u}_T \tag{15a}$$

$$\frac{\partial L_T^{HW}}{\partial \boldsymbol{u}_{\partial T}} \delta \boldsymbol{u}_{\partial T} = \int_{\partial_N T} (\boldsymbol{\theta}_{\partial T} - \boldsymbol{t}_{\partial_N T}) \cdot \delta \boldsymbol{u}_{\partial T} \qquad \forall \delta \boldsymbol{u}_{\partial T} \tag{15b}$$

$$\frac{\partial L_T^{HW}}{\partial \underset{\sim}{G}_T} \delta \underset{\sim}{G}_T = \int_T (\frac{\partial \psi_\Omega}{\partial \underset{\sim}{G}_T} - \underset{\sim}{P}_T) : \delta \underset{\sim}{G}_T \qquad \forall \delta \underset{\sim}{G}_T \tag{15c}$$

$$\frac{\partial L_T^{HW}}{\partial \underset{\sim}{P}_T} \delta \underset{\sim}{P}_T = \int_T (\nabla \boldsymbol{u}_T - \underset{\sim}{G}_T) : \delta \underset{\sim}{P}_T + \int_{\partial T} (\boldsymbol{u}_{\partial T} - \boldsymbol{u}_T|_{\partial T}) \cdot \delta \underset{\sim}{P}_T|_{\partial T} \cdot \boldsymbol{n} \qquad \forall \delta \underset{\sim}{P}_T \tag{15d}$$

where we introduced the *reconstructed traction force* $\boldsymbol{\theta}_{\partial T} = \underset{\sim}{P}_T|_{\partial T} \cdot \boldsymbol{n} + (\beta/h_T)(\boldsymbol{u}_{\partial T} - \boldsymbol{u}_T|_{\partial T})$. In particular, (15a) is the expression of the Principle of Virtual Work in T, where the *reconstructed traction force* $\boldsymbol{\theta}_{\partial T}$ replaces the usual expression $\underset{\sim}{P}_T \cdot \boldsymbol{n}$ in the external contribution. (15b) denotes a supplementary equation to the usual continuous problem as described in (8), to account for the continuity of the flux $\boldsymbol{\theta}_{\partial T}$ across the cell boundary. (15c) accounts for the constitutive equation in a weak sense, and (15d) defines the equation of an enhanced gradient field, that does not reduce to the projection of $\nabla \boldsymbol{u}_T$ as in (8c), since it is enriched by a boundary component that depends on the displacement jump. This feature is at the origin of the robustness of non-conformal methods to volumetric locking (see Appendix A.2 for more details on this note).

3.4. Problem in primal form

Reconstructed gradient. Since minimization of (15d) defines a linear problem with any displacement pair $(v_T, v_{\partial T})$, one can eliminate (15d) from the system (15). The resulting equation defines the so-called *reconstructed gradient* $\underset{\sim}{G}_T(v_T, v_{\partial T})$ associated with any displacement pair $(v_T, v_{\partial T})$, that solves

$$\int_T \underset{\sim}{G}_T : \underset{\sim}{\tau}_T = \int_T \nabla v_T : \underset{\sim}{\tau}_T + \int_{\partial T} (v_{\partial T} - v_T|_{\partial T}) \cdot \underset{\sim}{\tau}_T|_{\partial T} \cdot n \quad \forall \underset{\sim}{\tau}_T \tag{16}$$

where $\underset{\sim}{\tau}_T$ denotes an arbitrary kinematically admissible stress field.

Stress tensor. Likewise, (15c) is eliminated from (15) since it is linear with $\underset{\sim}{G}_T$. Assuming in addition that the space of kinematically admissible stress fields is included in that of kinematically admissible displacement gradient fields, (15c) holds in a strong sense such that

$$\underset{\sim}{P}_T = \frac{\partial \psi_\Omega}{\partial \underset{\sim}{G}_T} \tag{17}$$

Total Lagrangian for the problem in primal form. By elimination of both (15c) and (15d) from (15), the only remaining unknowns are the cell and boundary displacement fields. Hence, a new Lagrangian that accounts for the problem in primal form arises from (14).

$$L_T^{VW} = \int_T \psi_\Omega + \int_{\partial T} \frac{\beta}{2h_T} \|u_{\partial T} - u_T|_{\partial T}\|^2 - \int_T f_V \cdot u_T - \int_{\partial_N T} t_{\partial_N T} \cdot u_{\partial T} \tag{18}$$

Principle of virtual works for HDG methods. Minimization of the Lagrangian (18) amounts to the definition of a Principle of Virtual Work, in the context of HDG methods. It consists in finding the displacement pair $(u_T, u_{\partial T})$ that solves

$$\delta L_{T,\text{int}}^{VW}((u_T, u_{\partial T}), (\delta u_T, \delta u_{\partial T})) - \delta L_{T,\text{ext}}^{VW}(\delta u_T, \delta u_{\partial T}) = 0 \qquad \forall (\delta u_T, \delta u_{\partial T}) \tag{19}$$

with

$$\delta L_{T,\text{int}}^{VW} = \int_T \underset{\sim}{P}_T(\underset{\sim}{G}_T(u_T, u_{\partial T})) : \underset{\sim}{G}_T(\delta u_T, \delta u_{\partial T}) + \int_{\partial T} (\beta/h_T) Z_{\partial T}(u_T, u_{\partial T}) \cdot Z_{\partial T}(\delta u_T, \delta u_{\partial T}) \tag{20a}$$

$$\delta L_{T,\text{ext}}^{VW} = \int_{\partial_N T} t_{\partial_N T} \cdot \delta u_{\partial T} + \int_T f_V \cdot \delta u_T \tag{20b}$$

where we introduced the jump function $Z_{\partial T}$ such that

$$Z_{\partial T}(v_T, v_{\partial T}) = v_{\partial T} - v_T|_{\partial T} \quad \forall (v_T, v_{\partial T}) \tag{21}$$

In particular, one can readliy see the resemblance of (20) with (6), where the so called *reconstructed gradient* $\underset{\sim}{G}_T(u_T, u_{\partial T})$ plays the role of the usual displacement Lagrangian gradient ∇u_T, and where an additional *stabilization term* corresponding to a traction energy on the boundary has been added to account for the penalization of the displacement jump on ∂T through $Z_{\partial T}$ (or, equivalently, to account for the infinitesimal interface that lays between the bulk domain and its boundary). Equations (18), (16) and (17) define the mechanical problem to solve at the cell level for HDG methods, and (19) describes the weak form of these equations.

3.5. Small strain hypothesis

The proposed large deformation formulation also allows a natural transition to the small deformation framework. In this context, since the gradient of the transformation $\underset{\sim}{F}_T$ is assumed to be small compared to $\underset{\sim}{1}$, we seek the

infinitesimal deformation field $\underset{\sim}{\varepsilon}_T$ as the weak formulation of $\nabla^s \boldsymbol{u}_T$ rather than the gradient of the displacement field $\boldsymbol{G}_T$. The stress tensor $\boldsymbol{P}_T$ is then identified with the Cauchy stress $\underset{\sim}{\sigma}_T$, so that problem (14) becomes

$$
\begin{aligned}
L_T^{HW} = \int_T \psi_\Omega + (\nabla^s \boldsymbol{u}_T - \underset{\sim}{\varepsilon}_T) : \underset{\sim}{\sigma}_T + \int_{\partial T} (\boldsymbol{u}_{\partial T} - \boldsymbol{u}_T|_{\partial T}) \cdot \underset{\sim}{\sigma}_T|_{\partial T} \cdot \boldsymbol{n} + \int_{\partial T} \frac{\beta}{2h_T} \|\boldsymbol{u}_{\partial T} - \boldsymbol{u}_T|_{\partial T}\|^2 \\
- \int_T \boldsymbol{f}_V \cdot \boldsymbol{u}_T - \int_{\partial_N T} \boldsymbol{t}_{\partial_N T} \cdot \boldsymbol{u}_{\partial T}
\end{aligned}
\tag{22}
$$

Continuing the same development as above, the energy to be minimized is given by equation 18 as in the large deformation framework. On the other hand, the reconstructed gradient equation 16 becomes

$$
\int_T \underset{\sim}{\varepsilon}_T(\boldsymbol{v}_T, \boldsymbol{v}_{\partial T}) : \underset{\sim}{\tau}_T = \int_T \nabla^s \boldsymbol{v}_T : \underset{\sim}{\tau}_T + \int_{\partial T} (\boldsymbol{v}_{\partial T} - \boldsymbol{v}_T|_{\partial T}) \cdot \underset{\sim}{\tau}_T|_{\partial T} \cdot \boldsymbol{n} \quad \forall \underset{\sim}{\tau}_T
\tag{23}
$$

where $\underset{\sim}{\tau}_T$ deotes an arbitrary kinematically admissible symmetric stress field, since the deformations $\underset{\sim}{\varepsilon}_T$ and the Cauchy stress $\underset{\sim}{\sigma}_T$ are symmetric. The expression of the stress as a function of the cell deformation is then given by

$$
\underset{\sim}{\sigma}_T = \frac{\partial \psi_\Omega}{\partial \underset{\sim}{\varepsilon}_T}
\tag{24}
$$

3.6. Extension to the axi-symmetric framework

In the following section, we devise a Hybrid High order method for an axi-symmetric framework. Owing to geometrical assumptions on the displacement and its gradient, the definition of the reconstructed gradient (16) and of that of the higher order displacement (29) needs be modified accordingly. Details about the definitions of these ingredients can be found in Appendix A.3.

Axi-symmetric framework. The cartesian space is expressed in cylindrical coordinates and a point $X \in \Omega$ has coordinates $X = (r, z, \theta)$ where r denotes the radial component, z the ordinate one, and θ is the angular component describing a revolution around the axis $r = 0$. By cylindrical symmetry, the angular displacement u_θ is supposed to be zero, and both components u_r and u_z do not depend on the angular coordinate θ.

Axis faces treatment. Since in cylindrical coordinates, all integrals depend on the radial component r, boundary integrals vanish at $r = 0$ on the symmetry axis. Therefore, the reconstructed gradient (and the stabilization) do not depend on a closed surface wrapping a cell T located on the symmetry axis. However, this feature is necessary to prove the robustness of the HHO method to volumetric locking (see Appendix A.2). Therefore, in order to restore full mobility of a face located on the symmetry axis, we consider infinitely thin cylindrical faces wrapping it, that are subjected to Dirichlet boundary conditions along the radial direction.

4. Discretization

In this section, we specify the nature of the mesh, and introduce the so-called *skeleton* of the mesh, that bears boundary displacement unknowns. We then devise the problem to solve at the structural level, from the equilibrium of an element as described in Section 3.4. Approximation spaces for unknowns of the global problem are then described, which leads to several choices in terms of definition of the stabilization. Depending on such a choice, one recovers either the HDG method, or the HHO one. Finally, we give the expression of the global problem in discrete form.

4.1. Spatial discretization

Faces and skeleton of the mesh. The boundary ∂T of each element is decomposed in faces, such that a face F is a subset of Ω, and either there are two cells T and T' such that $F = \partial T \cap \partial T'$ (F is then an interior face), or there is a single cell T such that $F = \partial T \cap \partial \Omega$ (F is then an exterior face). For any cell T, let $\mathcal{F}(T) = \{F \in \mathcal{F} \mid F \subset \partial T\}$ the set of faces composing the boundary of T. Let finally $\mathcal{F}(\Omega) = \{F_i \subset \Omega \mid 1 \le i \le N_F\}$ the skeleton of the mesh, collecting all element faces F_i in the mesh, where N_F denotes the number of faces. The set of faces subjected to Neumann boundary conditions is denoted $\mathcal{F}_N^e(\Omega)$, and $\mathcal{F}_D^e(\Omega)$ denotes that subjected to Dirichlet boundary conditions.

Mesh description. Likewise, one defines the collection of all cells in the mesh as $\mathcal{T}(\Omega) = \{T_i \subset \Omega \mid 1 \leq i \leq N_T\}$, where N_T denotes the total number of cells. The composition of both $\mathcal{T}(\Omega)$ and $\mathcal{F}(\Omega)$ forms the hybrid mesh $\bar{\mathcal{T}}(\Omega) = \{\mathcal{T}(\Omega), \mathcal{F}(\Omega)\}$.

4.2. Global continuous problem

Global unknown. Let the global unknown $(v_{\mathcal{T}}, v_{\mathcal{F}})$ a displacement pair such that for each $T \in \mathcal{T}(\Omega), v_{\mathcal{T}} = v_T$ in T and for each $F \in \mathcal{F}(\Omega), v_{\mathcal{F}} = v_F$ on F, where v_T and v_F denote a cell and a face displacement field respectively.

Global weak form. The weak form of the global mechanical problem in Ω reads : find the global displacement unknown pair $(u_{\mathcal{T}}, u_{\mathcal{F}})$ verifying $u_{\mathcal{F}}|_{\partial_D \Omega} = u_D$ on $\partial_D \Omega$ such that $\forall (\delta u_{\mathcal{T}}, \delta u_{\mathcal{F}})$

$$\delta L_{\mathcal{T},\text{int}}^{VW} - \delta L_{\mathcal{T},\text{ext}}^{HW} = 0 \tag{25}$$

with

$$\delta L_{\mathcal{T},\text{int}}^{VW} = \sum_{T \in \mathcal{T}(\Omega)} \int_T \underset{\sim}{P}_T(\underset{\sim}{G}_T(u_T, u_{\partial T})) : \underset{\sim}{G}_T(\delta u_T, \delta u_{\partial T}) + \int_{\partial T} (\beta/h_T) Z_{\partial T}(u_T, u_{\partial T}) \cdot Z_{\partial T}(\delta u_T, \delta u_{\partial T}) \tag{26a}$$

$$\delta L_{\mathcal{T},\text{ext}}^{HW} = \sum_{F \in \mathcal{F}_N^e(\Omega)} \int_F t_N \cdot \delta u_F + \sum_{T \in \mathcal{T}(\Omega)} \int_T f_V \cdot \delta u_T \tag{26b}$$

where for each element $T \in \mathcal{T}(\Omega)$, the boundary displacement field $v_{\partial T}$ is such that $v_{\partial T} = v_F$ on F for every $F \in \mathcal{F}(T)$

4.3. Functional discretization and stabilization

Discrete functional space. For each element $T \in \mathcal{T}(\Omega)$, we denote $U^h(T)$ the approximation displacement space in the cell, and $V^h(\partial T)$ that on the boundary. Similarly, let $G^h(T)$ the space used to build the discrete reconstructed gradient and $S^h(T)$ that chosen for the discrete stress such that

$$U^h(T) = P^l(T, \mathbb{R}^d)$$
$$V^h(\partial T) = P^k(\partial T, \mathbb{R}^d)$$
$$G^h(T) = P^k(T, \mathbb{R}^{d \times d})$$
$$S^h(T) = P^k(T, \mathbb{R}^{d \times d})$$

where the cell displacement polynomial order l might be chosen different from the face displacement order k such that $k - 1 \leq l \leq k + 1$.

HDG stabilization. Accounting for the possible different polynomial order between the cell and faces, one can specify a discrete jump function in a natural way such that it delivers the displacement difference point-wise for any displacement pair $(v_T^l, v_{\partial T}^k) \in U^h(\bar{T})$

$$Z_{\partial T}^{HDG}(v_T^l, v_{\partial T}^k) = \Pi_{\partial T}^k (v_{\partial T}^k - v_T^l|_{\partial T}) \tag{27}$$

where $U^h(\bar{T}) = U^h(T) \times V^h(\partial T)$ and $\Pi_{\partial T}^k$ denotes the orthogonal projector onto $V^h(\partial T)$. This straightforward discrete jump function is at the origin of Hybrid Discontinuous Galerkin methods, and grants a convergence of order k in the energy norm.

HHO stabilization. A richer discrete jump function $Z_{\partial T}^{HHO}$ providing a convergence of order $k + 1$ in the energy norm was introduced in [42], hence giving the Hybrid High Order method its name, such that

$$Z_{\partial T}^{HHO}(v_T^l, v_{\partial T}^k) = \Pi_{\partial T}^k (v_{\partial T}^k - v_T^l|_{\partial T} - ((I_T^{k+1} - \Pi_T^k)(w_T^{k+1}))|_{\partial T}) \tag{28}$$

where Π_T^k is the projector onto $P^k(T, \mathbb{R}^d)$, I_T^{k+1} is the identity function in $D^h(T) = P^{k+1}(T, \mathbb{R}^d)$.

Reconstructed higher order displacement. The term w_T^{k+1} in (28) denotes a higher order discrete displacement in $D^h(T)$ that solves for any displacement pair $(v_T^l, v_{\partial T}^k) \in U^h(\bar{T})$

$$\int_T \nabla w_T^{k+1} : \nabla d_T^{k+1} = \int_T \nabla v_T^l : \nabla d_T^{k+1} + \int_{\partial T} (v_{\partial T}^k - v_T^l) \cdot \nabla d_T^{k+1} \cdot n \qquad \forall d_T^{k+1} \in D^h(T) \tag{29a}$$

$$\int_T w_T^{k+1} = \int_T v_T^l \tag{29b}$$

4.4. Global discrete problem

Discrete global approximtion spaces. Let $U^h(\mathcal{T}) = \prod_{T \in \mathcal{T}(\Omega)} U^h(T)$ the global discrete cell displacement space. Let $V^h(\mathcal{F}) = \prod_{F \in \mathcal{F}(\Omega)} V^h(F)$ the global discrete face displacement space, and $U^h(\bar{\mathcal{T}}) = U^h(\mathcal{T}) \times V^h(\mathcal{F})$ the global unknown approximation space.

Discrete global problem. The global problem in discrete form writes : find the pair $(u_{\mathcal{T}}^l, u_{\mathcal{F}}^k) \in U^h(\bar{\mathcal{T}})$ verifying $u_{\mathcal{F}}^k|_{\partial_D \Omega} = u_D$ on $\partial_D \Omega$ such that $\forall (\delta u_{\mathcal{T}}^l, \delta u_{\mathcal{F}}^k)$

$$\delta L_{\mathcal{T},\text{int}}^{HHO} - \delta L_{\mathcal{T},\text{ext}}^{HHO} = 0 \tag{30}$$

with

$$\delta L_{\mathcal{T},\text{int}}^{HHO} = \sum_{T \in \mathcal{T}(\Omega)} \int_T \underset{\sim}{P}_T^k (\underset{\sim}{G}_T^k(u_T^l, u_{\partial T}^k)) : \underset{\sim}{G}_T^k(\delta u_T^l, \delta u_{\partial T}^k) + \int_{\partial T} (\beta/h_T) Z_{\partial T}^{HHO}(u_T^l, u_{\partial T}^k) \cdot Z_{\partial T}^{HHO}(\delta u_T^l, \delta u_{\partial T}^k) \tag{31a}$$

$$\delta L_{\mathcal{T},\text{ext}}^{HHO} = \sum_{F \in \mathcal{F}_N^e(\Omega)} \int_F t_N \cdot \delta u_F^k + \sum_{T \in \mathcal{T}(\Omega)} \int_T f_V \cdot \delta u_T^l \tag{31b}$$

where the discrete reconstructed gradient $\underset{\sim}{G}_T^k(v_T^l, v_{\partial T}^k) \in G^h(T)$ solves $\forall (v_T^l, v_{\partial T}^k) \in U^h(\bar{T})$

$$\int_T \underset{\sim}{G}_T^k(v_T^l, v_{\partial T}^k) : \underset{\sim}{\tau}_T^k = \int_T \nabla v_T^l : \underset{\sim}{\tau}_T^k + \int_{\partial T} (v_{\partial T}^k - v_T^l|_{\partial T}) \cdot \underset{\sim}{\tau}_T^k|_{\partial T} \cdot n \quad \forall \underset{\sim}{\tau}_T^k \in S^h(T) \tag{32}$$

5. Implementation

In this section, we specify the underlying matricial implementation of problem (31). In the following, the expression $\{\cdot\}$ denotes a real-valued vector, and the notation $[\cdot]$ a real-valued matrix.

Quadrature. As is customary with finite element methods, integrals are evaluated numerically by means of a quadrature rule on an element shape. Hence, let Q_T a quadrature rule for the cell T of order at least $2k$. A quadrature point is denoted X_q and a quadrature weight w_q.

5.1. Reconstructed gradient and stabilization operators

Reconstructed gradient operator. From an algebraic standpoint, (32) defines a linear problem consisting in inverting a mass matrix in $G^h(T)$. One can thus defines $[B_T]$ the discrete gradient operator acting on the pair (v_T^l, v_T^k) at a quadrature point $X_q \in Q_T$ to evaluate the discrete gradient $\underset{\sim}{G}_T^k(v_T^l, v_{\partial T}^k)$ such that

$$\left\{ \underset{\sim}{G}_T^k(v_T^l, v_{\partial T}^k) \right\}(X_q) = \left[B_T \right](X_q) \cdot \begin{Bmatrix} v_T^l \\ v_{\partial T}^k \end{Bmatrix} \quad \forall (v_T^l, v_{\partial T}^k) \in U^h(\bar{T}) \tag{33}$$

where $[B_T]$ is composed by a cell block and a boundary block.

Stabilization operator. Similarly, the algebraic realization of (28) amounts to compute the stabilization operator $[Z_T]$ such that

$$\left\{ Z_{\partial T}^{HHO}(v_T^l, v_{\partial T}^k) \right\} = \left[Z_T \right] \cdot \begin{Bmatrix} v_T^l \\ v_{\partial T}^k \end{Bmatrix} \quad \forall (v_T^l, v_{\partial T}^k) \in U^h(\bar{T}) \tag{34}$$

as for $[B_T]$, the operator $[Z_T]$ is composed by a cell and a boundary block.

Offline computation. Since (32) and (28) depend on the geometry of the element T only, one can compute the operators $[B_T]$ and $[Z_T]$ for each element once and for all in an offline pre-computation step by working in the reference configuration. Once this offline step is performed, the algebraic form of the problem resembles closely to the standard finite element one, where the operator $[B_T]$ replaces the usual shape function gradient operator, and the stabilization operator $[Z_T]$ is incorporated in the expression of the tangent matrix and in that of internal forces.

5.2. Iterative method

Notations. In the following, let $(\boldsymbol{u}_T^{l,m,n}, \boldsymbol{u}_{\partial T}^{k,m,n})$ denote the displacement pair value at some pseudo time step m and some iteration n. The initial value of the displacement at time step $m = 0$ and iteration $n = 0$ is set to zero, and at a new pseudo time step $m + 1$, the displacement at the first iteration $n = 0$ takes the value of the displacement of the last iteration of the previous time step.

Internal forces. In such a context, the internal forces vector $\{F_T^{int}(\boldsymbol{u}_T^{l,m,n}, \boldsymbol{u}_{\partial T}^{k,m,n})\}$ writes

$$\left\{F_T^{int}(\boldsymbol{u}_T^{l,m,n}, \boldsymbol{u}_{\partial T}^{k,m,n})\right\} = \sum_{X_q \in Q_T} \left[B_T\right]^{\text{trans}}(X_q) \cdot \left\{\underset{\sim}{\boldsymbol{P}}_T^k(\underset{\sim}{\boldsymbol{G}}_T^k(\boldsymbol{u}_T^{l,m,n}, \boldsymbol{u}_{\partial T}^{k,m,n}))\right\}(X_q) + \frac{\beta}{h_T}\left[Z_T\right]^{\text{trans}} \cdot \left[Z_T\right] \cdot \left\{\begin{matrix} \boldsymbol{u}_T^{l,m,n} \\ \boldsymbol{u}_{\partial T}^{k,m,n}\end{matrix}\right\} \tag{35}$$

where the superscript $[\cdot]^{\text{trans}}$ denotes the transpose operation, and $\{\underset{\sim}{\boldsymbol{P}}_T^k(\underset{\sim}{\boldsymbol{G}}_T^k(\boldsymbol{u}_T^{l,m,n}, \boldsymbol{u}_{\partial T}^{k,m,n}))\}$ is the stress components vector, computed by integration of the behavior law at each quadrature point X_q from the values of the displacement gradient $\underset{\sim}{\boldsymbol{G}}_T^k(\boldsymbol{u}_T^{l,m,n}, \boldsymbol{u}_{\partial T}^{k,m,n})$.

External forces. The external forces vector is, as is customary with the standard finite element method, the evaluation of the given bulk and boundary loads at respective cell and face quadrature points tested against the respective cell and face shape functions, and is denoted

$$\left\{F_T^{ext}\right\} = \left\{\begin{matrix} \boldsymbol{f}_V \\ \boldsymbol{t}_N\end{matrix}\right\} \tag{36}$$

Tangent matrix. The tangent matrix $[K_T^{tan}(\boldsymbol{u}_T^{l,m,n}, \boldsymbol{u}_{\partial T}^{k,m,n})]$ is the sum of the usual product of the displacement gradients by the tangent operator $\underset{\approx}{\boldsymbol{A}}(\boldsymbol{u}_T^{l,m,n}, \boldsymbol{u}_{\partial T}^{k,m,n})$ and of an additional stabilization term such that

$$\left[K_T^{tan}(\boldsymbol{u}_T^{l,m,n}, \boldsymbol{u}_{\partial T}^{k,m,n})\right] = \sum_{X_q \in Q_T} \left[B_T\right]^{\text{trans}}(X_q) \cdot \left[\underset{\approx}{\boldsymbol{A}}(\boldsymbol{u}_T^{l,m,n}, \boldsymbol{u}_{\partial T}^{k,m,n})\right](X_q) \cdot \left[B_T\right](X_q) + \frac{\beta}{h_T}\left[Z_T\right]^{\text{trans}} \cdot \left[Z_T\right] \tag{37}$$

where $\underset{\approx}{\boldsymbol{A}}(\boldsymbol{u}_T^{l,m,n}, \boldsymbol{u}_{\partial T}^{k,m,n})$ is the derivative of the stress with respect to the displacement gradient

$$\underset{\approx}{\boldsymbol{A}}(\boldsymbol{u}_T^{l,m,n}, \boldsymbol{u}_{\partial T}^{k,m,n}) = \frac{\partial \underset{\sim}{\boldsymbol{P}}_T^k}{\partial \underset{\sim}{\boldsymbol{G}}_T^k} \tag{38}$$

Newton method. Following the iterative Newton method, the algebraic system to solve at the element level consists in finding the displacement increment $(\delta\boldsymbol{u}_T^l, \delta\boldsymbol{u}_{\partial T}^k)$ that solves

$$-\left[K_T^{tan}(\boldsymbol{u}_T^{l,m,n}, \boldsymbol{u}_{\partial T}^{k,m,n})\right] \cdot \left\{\begin{matrix} \delta\boldsymbol{u}_T^l \\ \delta\boldsymbol{u}_{\partial T}^k\end{matrix}\right\} = \left\{R_T^{m,n}\right\} \quad \text{with} \quad \left\{R_T^{m,n}\right\} = \left\{F_T^{int}(\boldsymbol{u}_T^{l,m,n}, \boldsymbol{u}_{\partial T}^{k,m,n})\right\} - \left\{F_T^{ext}\right\} \tag{39}$$

such that the displacement at the next iteration is incremented by the displacement increment $(\delta\boldsymbol{u}_T^l, \delta\boldsymbol{u}_{\partial T}^k)$

$$\left\{\begin{matrix} \boldsymbol{u}_T^{l,m,n+1} \\ \boldsymbol{u}_{\partial T}^{k,m,n+1}\end{matrix}\right\} = \left\{\begin{matrix} \boldsymbol{u}_T^{l,m,n} \\ \boldsymbol{u}_{\partial T}^{k,m,n}\end{matrix}\right\} + \left\{\begin{matrix} \delta\boldsymbol{u}_T^l \\ \delta\boldsymbol{u}_{\partial T}^k\end{matrix}\right\} \tag{40}$$

5.3. Static condensation

Static condensation.   Since both $[B_T]$ and $[Z_T]$ are expressed in terms of cell and boundary blocks, so does the tangent matrix which can be decomposed into four coupled cell-boundary blocks with the notation

$$\left[K_T^{tan}(\boldsymbol{u}_T^{l,m,n}, \boldsymbol{u}_{\partial T}^{k,m,n})\right] = \begin{bmatrix} K_{TT}(\boldsymbol{u}_T^{l,m,n}, \boldsymbol{u}_{\partial T}^{k,m,n}) & K_{T\partial T}(\boldsymbol{u}_T^{l,m,n}, \boldsymbol{u}_{\partial T}^{k,m,n}) \\ K_{\partial TT}(\boldsymbol{u}_T^{l,m,n}, \boldsymbol{u}_{\partial T}^{k,m,n}) & K_{\partial T\partial T}(\boldsymbol{u}_T^{l,m,n}, \boldsymbol{u}_{\partial T}^{k,m,n}) \end{bmatrix} \tag{41}$$

Moreover, since $\underset{\approx}{\boldsymbol{A}}(\boldsymbol{u}_T^{l,m,n}, \boldsymbol{u}_{\partial T}^{k,m,n})$ is definite symmetric (and positive until an eventual loss of coercivity for *e.g.* high plastic deformations), the cell block K_{TT} is invertible and one can condensate it through a Schur complement step in order to eliminate the cell unknown, such that (39) expresses only in terms of boundary increment unknowns

$$-\left[K_T^{tan}(\boldsymbol{u}_T^{l,m,n}, \boldsymbol{u}_{\partial T}^{k,m,n})\right]_{\text{cond}} \cdot \left\{\delta\boldsymbol{u}_{\partial T}^k\right\} = \left\{F_T^{int}(\boldsymbol{u}_T^{l,m,n}, \boldsymbol{u}_{\partial T}^{k,m,n})\right\}_{\text{cond}} - \left\{F_T^{ext}\right\}_{\text{cond}} = \left\{R_T^{m,n}\right\}_{\text{cond}} \tag{42}$$

with

$$\left[K_T^{tan}\right]_{\text{cond}} = \left[K_{\partial T\partial T}\right] - \left[K_{\partial TT}\right] \cdot \left[K_{TT}\right]^{-1} \cdot \left[K_{T\partial T}\right] \quad \text{and} \quad \left\{R_T\right\}_{\text{cond}} = \left\{R_{\partial T}\right\} - \left[K_{\partial TT}\right] \cdot \left[K_{TT}\right]^{-1} \cdot \left\{R_T\right\} \tag{43}$$

and the incremental cell displacement expresses linearly with the respect to the boundary one such that

$$\left\{\delta\boldsymbol{u}_T^l\right\} = \left[K_{TT}\right]^{-1}\left(-\left\{R_T\right\} - \left[K_{T\partial T}\right] \cdot \left\{\delta\boldsymbol{u}_{\partial T}^k\right\}\right) \tag{44}$$

5.4. Algorithmic aspects

Linear static condensation algorithm.   At a given pseudo-time step m and iteration n, the element displacement unknown is incremented by the element displacement increment. The reconstructed gradient field is then computed, and is used to integrate the behaviour law, which provides the stress and tangent operator values at quadrature points. The internal forces, external forces and tangent matrix are then computed, and condensated on the element faces. The resulting system is assembled on the global system matrix, and a new value of the increment is computed by inverting the global matrix. A schematic representation this procedure is given in Figure 2
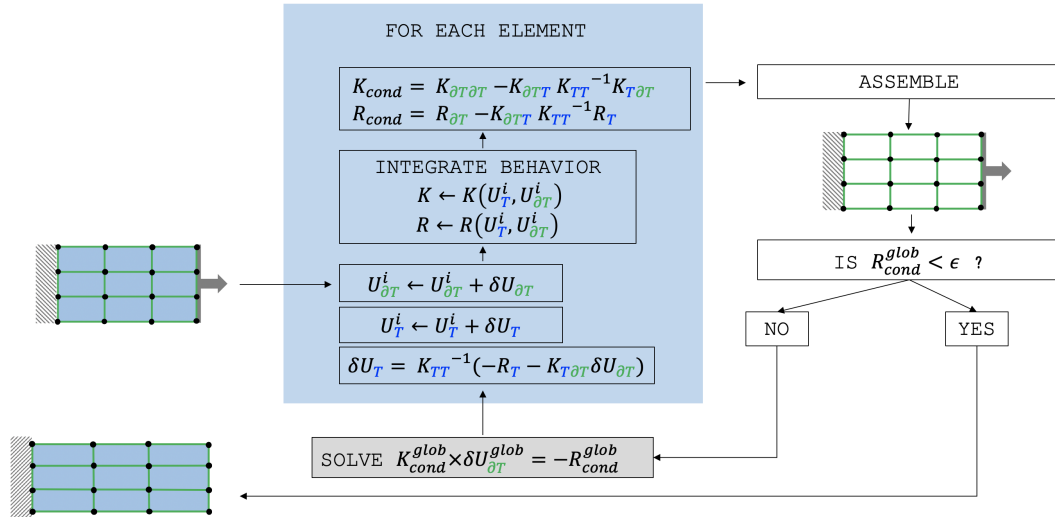

Figure 2.   schematic description of the Linear static condensation algorithm

Cell equlibrium algorithm. We propose an alternative to the static condensation solving algorithm, postulating an implicit relation between the increment of the cell unknowns and the increment of the faces, that consists in solving locally a nonlinear system on the cell increment at a fixed face increment. This non-linear local procedure adds up to the algorithm described above, to ensure the equilibrium of the cell with its faces at each iteration of the global problem. This new solution scheme is described in Figure 3, where we note i a Newton iteration for solving the global problem on the set of face unknowns, and j a Newton iteration for solving the local problem on the cell unknowns in an element.
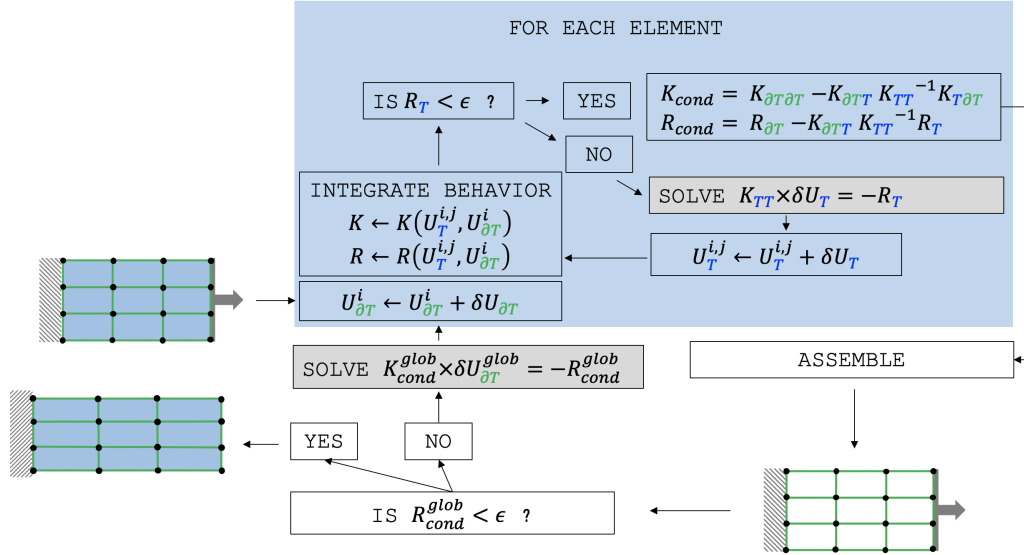

Figure 3. schematic description of the Linear Cell equilibrium algorithm

Comparison of both algorithms. The Linear static condensation algorithm is the one described in the literature [42, 43, 44, 45] to condensate cell unknowns on faces. This procedure needs not iterate at the cell level to acomodate the cell increment, and is hence, faster. However, one needs to store matrices used during the condensation step from one iteration to another in order do decondensate the cell increment.

The Cell equlibrium algorithm, needs iterate at the cell level. It is hence is more costly, and requires to integrate the behaviour law more times that does the Linear static condensation algorithm. However, it allows to consider extending the present non-linear algorithm to *e.g.* constrained resolution algorithm, to solve inequality constrained problems, as encountered in multi-field plasticity [46] for instance.

6. Numerical examples in the Axisymmetric framework

In this section, we evaluate the proposed axi-symmetric HHO method on classical test cases taken from the literature to emphasize robustness to volumetric locking. We consider both the small and large strains framework, for elasto-plastic behaviors. In this section, we denote by HHO(k, l) the HHO element of order k on faces, and order l in the cell.

Stabilization parameter. To ensure coercivity of the HHO method, the stabilization parameter β needs be chosen according to the material under study. In the literature [42], a value of order 2μ is advocated, where μ denotes the shear modulus of the material. We use this values for all test cases in the present section.

6.1. The free dilatation test

The first test case of the following benchmark aims at displaying the robustness of the HHO method for coupled mechanical-thermal problems.

Specimen and loading. For this test case, the unit box is fixed on both the right and bottom boundaries in their respective normal directions, and a quadratic thermal load depending on the *r*-coordinate is imposed in the solid (see Figure 4). The mesh is composed of 400 quadrangles. The thermal loading is given by

$$T(r, z) = 4(T_{max} - T_{min})r(1 - r) + T_{min} \tag{45}$$

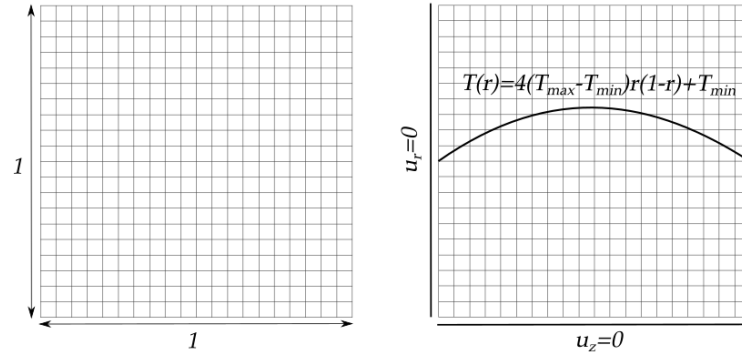with temperature values T_{max} = 2000 K and T_{min} = 293.15 K.

Figure 4. Geometry, displacement boundary conditions and temperature loading for the free dilatation test case

Material behaviour. A linear thermo-elastic energy potential is considered with a Young modulus E = 150 GPa. The material is quasi-incompressible with a Poisson ration ν = 0.499. The dilatation parameter is taken as $\alpha = 1e^{-6}$ K^{-1}.

Volumetric locking and polynomial approximation for the strain and temperature fields. Lagrange finite elements of order $1 \leq k \leq 2$ evaluate a mechanical strain of order $0 \leq k - 1 \leq 1$, whereas the thermal strain is of order 2. Using the total strain for the computation of the stress results in strong volumetric locking. Hence, for Lagrange element to accurately model the problem, one needs to choose a temperature fields that is one order lower than that describing the displacement field. This feature is of major importance for mixed elements, where quadratic elements needs be employed to match the the linear pressure unknown polynomial order.
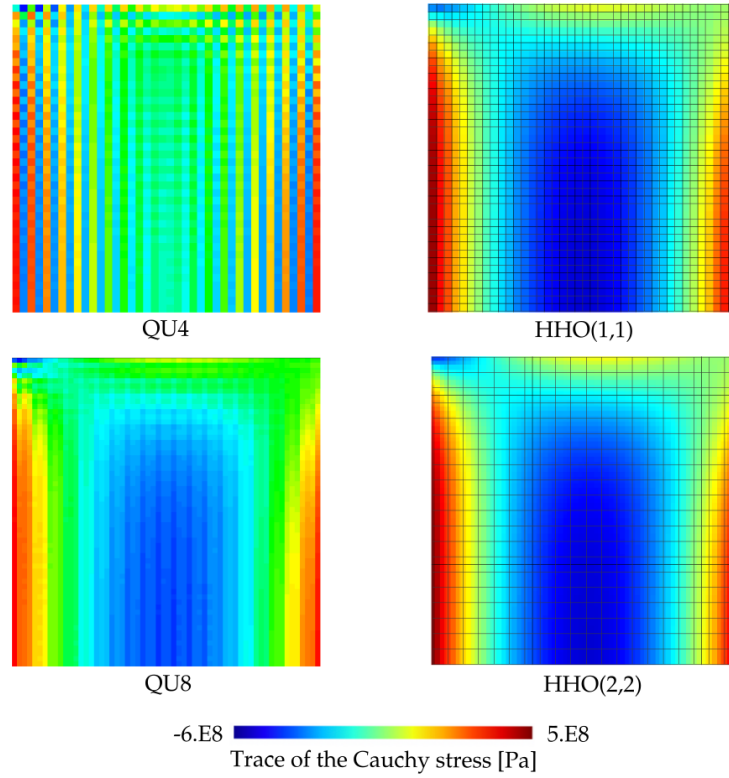
Figure 5. Map fo the Trace of the Cauchy stress at quadrature points for the Free dilatation test case at the last time step

Comparison of FE and HHO methods. In Figure 5, one can observe that the pressure map is completely smooth for the HHO computations, even for a quadratic temperature field acting on a linear gradient using HHO(1,1). As expected, the results display mild signs of volumetric locking for the quadratic finite element approximation, and strong oscillations are noted for the linear finite element solution.

6.2. Perfect plastic swelling sphere

Specimen and loading. This benchmark consists in a quasi-incompressible sphere under uniform internal loading. This test case has an analytical solution and the state of the specimen is known when the plastic region has reached the external border of the sphere. The sphere has an inner radius $r_{int} = 0.8$ mm and an outer radius $r_{ext} = 1$ mm. An internal radial displacement u is imposed. The mesh is composed of XXX quadrangles (see Figure 7). The simulation is performed until the limit load corresponding to an internal displacement of 0.2 mm is reached.

Material behaviour. An isotropic hardening energy potential ψ_Ω^p is chosen for the description of the plastic evolution of the material such that

$$\psi_\Omega^p(p) = \sigma_0 p + \frac{1}{2}Hp^2 + (\sigma_\infty - \sigma_0)(p - \frac{1 - e^{-\delta p}}{\delta}) \tag{46}$$

where the parameter p denotes the equivalent plastic strain and a Von Mises yields function f describes the flow rule

$$f = \sqrt{\frac{3}{2}}\|\text{dev}(\sigma)\| - p \tag{47}$$

Moreover, the small strain hypothesis is assumed for this test case.

16

Perfect plasticity is considered for this test case , where the saturation parameter $\delta = 0$, the yield stresses $\sigma_0 = \sigma_\infty = 6$ MPa, the hardening parameter $H = 0$ and the elastic potential parameters are the Young modulus $E = 28.85$ MPa and the Poisson ratio $\nu = 0.499$, such that the material is quasi-incompressible.
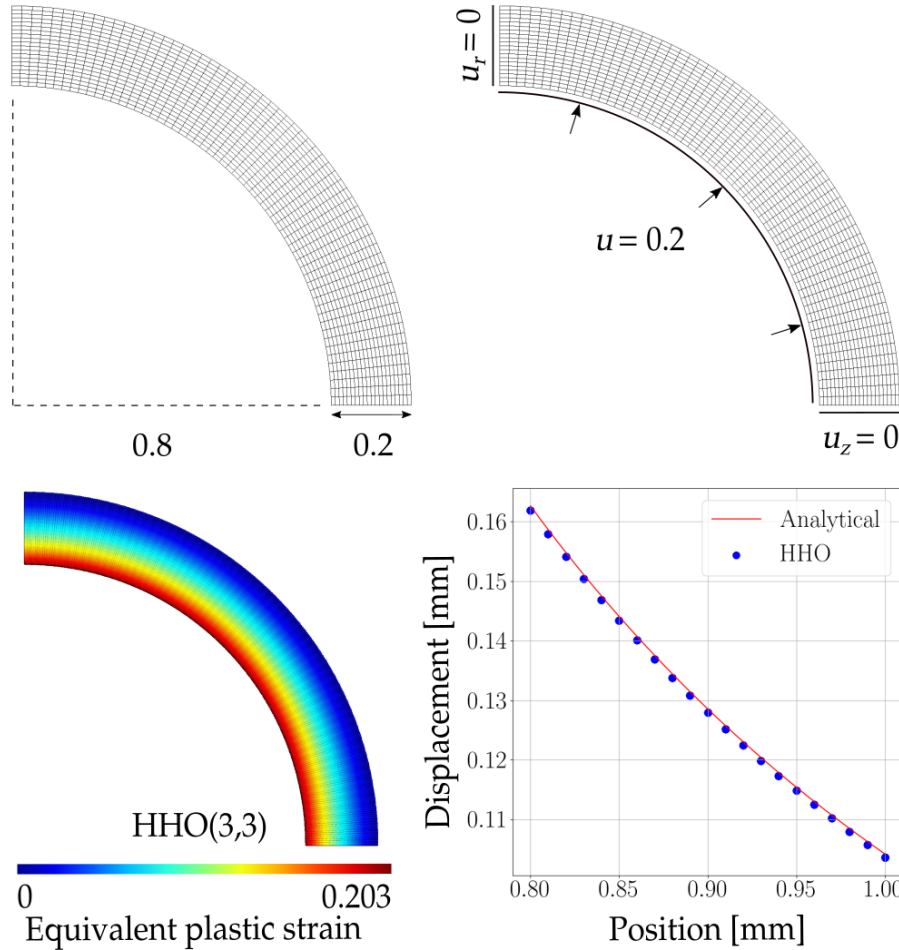

Figure 6. the swelling sphere test case. Geometry, loadings, final displacement along the radius of the sphere, and final equivalent plastic strain map at quadrature points

Displacement along the radius. Since an analytical solution is known for this test case, we compare it to the proposed HHO method. The displacement of the section of the sphere at cell nodes is plotted in Figure 7, along with the analytical one, and we observe that the obtained results are in agreement with the analytical response. Figure 7 mentions the label HHO without specifying approximation orders for all computations deliver the same result.

Trace of the Cauchy stress. As for the displacement, the analytical solution for the trace of the Cauchy stress tensor is compared to the one computed using the proposed HHO method for three approximation orders. A sign of volumetric locking is the presence of strong oscillations in the trace of the Cauchy stress (or, equivalently, the hyrostatic pressure) within elements. We observe that numerical results at quadrature points fit the analytical curve, and display no sign of volumetric locking. The computed solution is however less smooth at the borders of the specimen for higher orders, a phenomenon that was pointed out in [44] for the three dimensional case, and attributed to the fact that planar faces are considered.
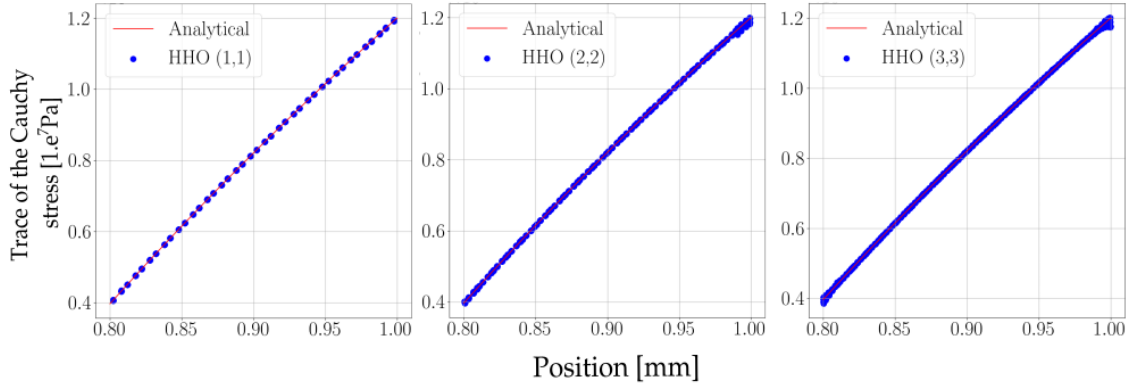
Figure 7. trace of the Cauchy stress tensor along the radius of the sphere at quadrature points

6.3. Necking of a notched bar

Specimen and loading. We consider a notched bar that is subjected to uniaxial extension. The bar has a length of 30 mm, a top section of radius 5 mm and a bottom section of radius 3 mm. A vertical displacement $u_z = 0.8$ mm is imposed at the top, as shown in Figure 9. For symmetry reasons, only one-quarter of the bar is discretized, and the mesh is composed of XXX quadrangles.

Behaviour law. The same behavior law as that in 6.2 is considered for the present test case. However, the finite strain hypothesis is chosen, based on a logarithmic decomposition of the stress [47].

Material parameters. Materials parameters are taken as $\sigma_0 = 450$ MPa, $\sigma_\infty = 715$ MPa with a saturation parameter $\delta = 16.93$. The Young modulus is $E = 206.9$ GPa, and the Poisson ratio is $\nu = 0.29$.

Load deflection curve. The load-displacement curve is plotted in Figure 9, and gives similar results to that obtained with quadratic reduced integration elements.

Equivalent plastic strain. Moreover, the equivalent plastic strain p at quadrature points and at the final load is plotted Figure 8. It has been observed that the equivalent plastic strain might suffer some oscillations at a certain limit load with UPG methods. One notices through the present example, that the proposed HHO method displays no oscillations of the equivalent plastic strain.

Figure 8. final equivalent plastic strain map at quadrature points in the notch region

Hydrostatic pressure. The hyrostatic pressure map at quadrature points and at the final load is shown Figure 9 for three HHO element orders (respectively 1, 2 and 3). As for the swelling sphere test case, one notices that the hydrostatic pressure map is fairly smooth over the whole structure at all approximation orders, even at the bottom left corner where plasticity is confined.

Figure 9. the notched specimen test case. Geometry, loadings, load deflection curve, and final hydrostatic pressure map at quadrature points in the notch region

7. Numerical examples using the cell resolution algorithm

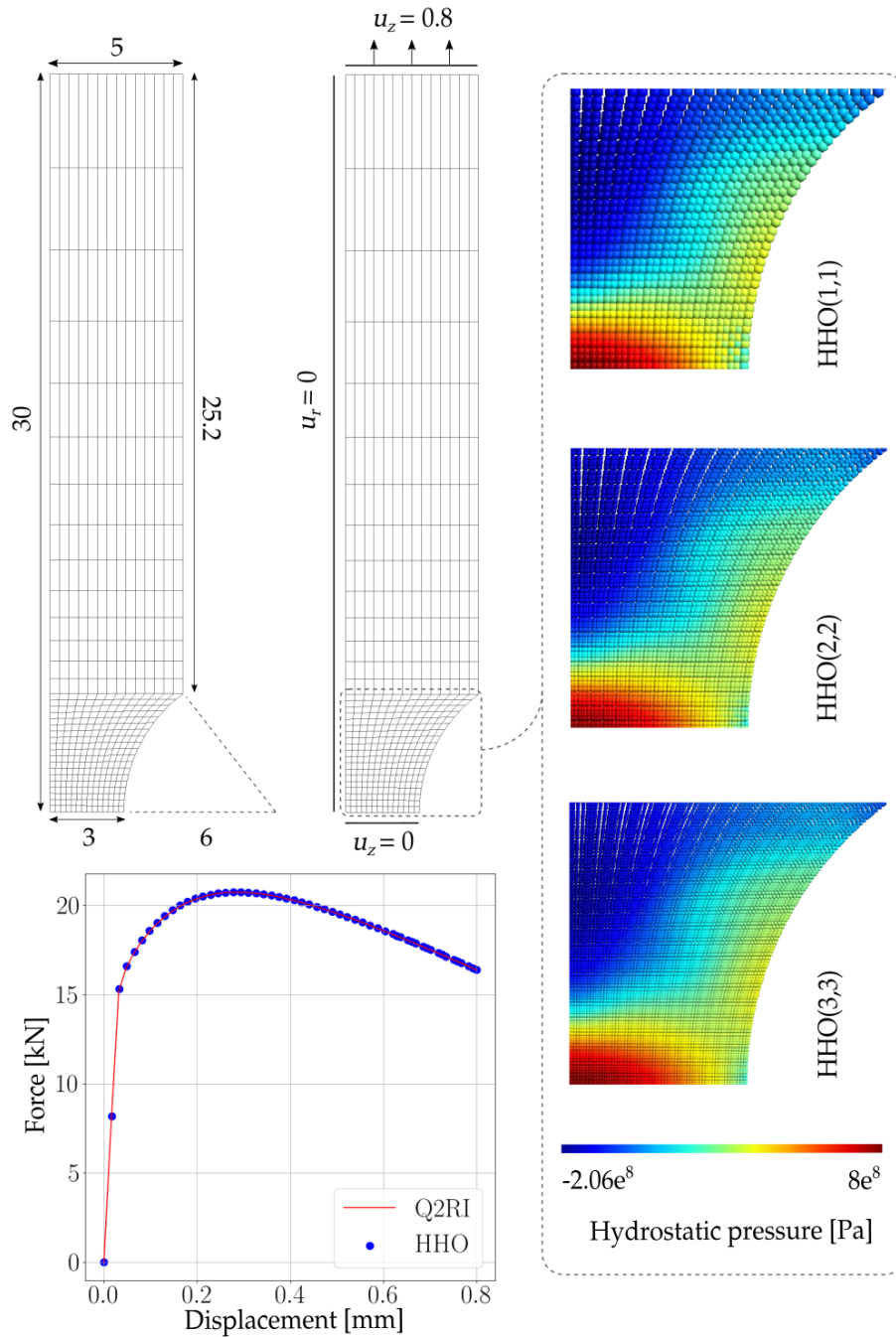The section showcases numerical examples demonstrating the robustness of the cell resolution algorithm. The test cases under study, namely the classical Cook membrane, and the indentation test cases, show that no volumetric locking is encountered using the cell resolution algorithm.

7.1. Cook's membrane test case

Specimen and loading. Let consider the Cook membrane specimen that is subjected to uniaxial traction. The membrane has a width of 48 mm and a height of 60 mm, and a vertical traction $t_y = 1000$ N/m is imposed at the top. The HHO computation is run on a polygonal mesh (see Figure 10) and is compared with standard QU4 and QU8 formulations (*i.e.* linear and quadratic approximations)

Constitutive equation. The same behavior law as that in 6.2 is considered for the present test case. However, the finite strain hypothesis is chosen, based on a logarithmic decomposition of the stress [47].

Material parameters. Materials parameters are taken as $\sigma_0 = 450$ MPa, $\sigma_\infty = 715$ MPa with a saturation parameter $\delta = 16.93$. The Young modulus is $E = 206.9$ GPa, and the Poisson ratio is $\nu = 0.29$.

-1.25E9   HYDROSTATIC PRESSURE [Pa]   3.98E8

Figure 10. Hydrostatic pressure map one the reference configuration at the limit load

Numerical results. As expected, the linear and quadratic finite element methods display respectively strong and mild oscillations of the pressure, whereas the HHO one shows no sign of locking.

7.2. Indentation test case

Specimen and loading. The last test case consists in the indentation of a cube of size 10 mm. A pressure of 300 MPa is imposed on the top surface see Figure 11).

Material. The same perfect plastic material as that in 6.2 is considered for the present test case.
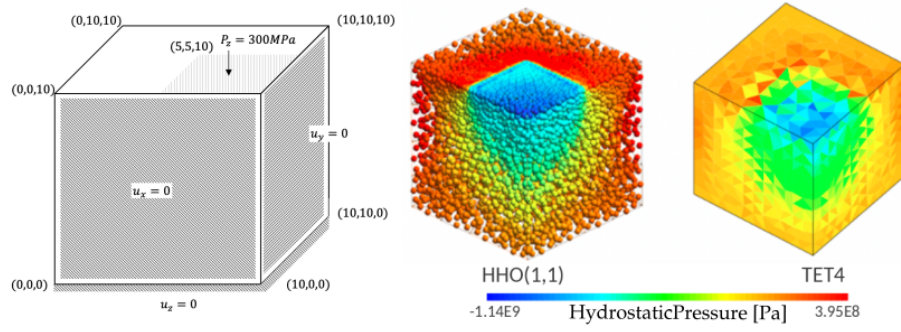
Figure 11. Hydrostatic pressure map one the reference configuration at the limit load

Numerical results. The pressure map at the end of the computation is displayed in Figure 11, and no sign of volumetric locking are present on the HHO computation, as opposed to the linear finite element one.

Performance of the algorithm. As stated in Section 5.4, the cell resolution algorithm needs more iterations (see Figure 12) than the classical linear resolution using a static condensation procedure. Indeed, since after a increment over the skeleton of the mesh, the cell displacement does not yet solve the equilibrium in the cell, the computation of the reconstructed gradient is not accurate, which results in ill-computed stresses at quadrature points. In order to circumvent this phenomenon, a prediction step is used to lift the cell displacement and then solve a non-linear problem within the cell. Using this prediction step displays similar results that those obtained with the static condensation algorithm (see Figure 12).

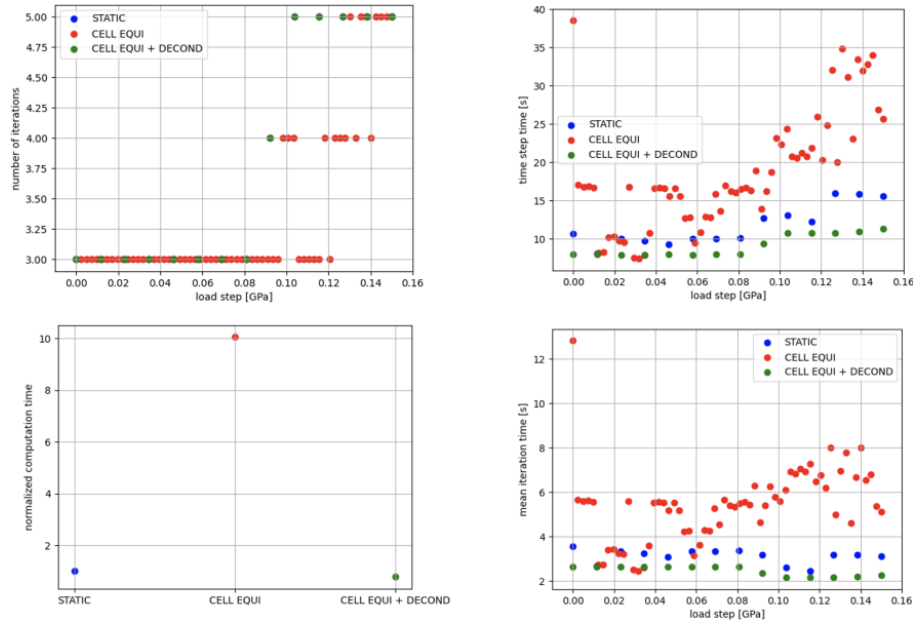Figure 12. Comparison in terms of performance for different algorithms

8. Conclusion

An introduction to HDG and HHO methods has been proposed, based on the minimization of a Hu-Washizu Lagrangian. The expression of the method arising from this approach allows to introduce naturally all the ingredients of the method, as well as the displacement discontinuity, in a unified framework. This new formulation also allows

one to draw a connection between HDG methods and other locking-free methods, all based on the minimization of a Hu-Washizu Lagrangian. A natural cell-based resolution scheme emerged from this formulation, leading to the proposition for a novel algorithm, based on the resolution of the equilibrium of the cell. This algorithm has been tested and investigated. Finally, we have devised and evaluated numerically an HHO method to account for mechanical problems in the axisymmetric framework, for both linear thermoelastic behaviours, and plastic behaviours under both the small and finite strain hypotheses. The HHO method exhibits a robust behavior for strain-hardening plasticity as well as for perfect plasticity and produces accurate solutions with a moderate number of degrees of freedom for various benchmarks from the literature.

This work can be pursued in several directions. One could use the cell resolution algorithm to address local resolution problems, such as those encountered with *e.g.* damage irreversibility in phase field fracture mechanics, or multi field plasticity. Moreover, an adaptation of the HHO method to reconstruct pressure-driven gradient terms only could lead to a simpler formulation, closer to that of mixed methods [38].

9. Aknowledgements

...

Appendix A. Appendix

Appendix A.1. From the continuous Hu-Washizu Lagrangian to the HDG Lagrangian

In this part, the development for the expression of the Hu-Washizu Lagrangian (14) is exposed, using the assumptions made in Section 3.2.

Element geometry. In the following, the cell T is assumed to be convex. It is split into a core part $K \subset T$ with boundary ∂K, and into an interface part $I \subset T$ with boundary $\partial I = \partial K \cup \partial T$, as shown in Figure 1. The interface I has some thickness $\ell > 0$ that is supposed to be small compared to h_T the diameter of T.

Homotethic transformation. Let $\mathbf{\Xi}_T$ the homothety of ratio $(1 - \alpha\ell)$ and center X_T the centroid of T, with $0 < \alpha < 1/\ell$ such that K (respectively ∂K) is the image of T (respectively ∂T) by $\mathbf{\Xi}_T$. Since ∂K is an homothety of ∂T, any point $X_{\partial T} \in \partial T$ and $X_{\partial K} = \mathbf{\Xi}_T(X_{\partial T}) \in \partial K$ share the same unit outward normal $\boldsymbol{n}$.

Change of reference. Let the change of frame $\mathbf{\Psi}$ that takes a point from the reference frame to the local frame with origin on ∂K, and whose first direction is given by the normal vector $\boldsymbol{n}$ such that

$$\mathbf{\Psi} : X \mapsto x = \underset{\sim}{Q}X + c \tag{A.1}$$

where $\underset{\sim}{Q}$ is the rotation matrix whose first row coincides with $\boldsymbol{n}$, and c is a constant vector.

Displacement in the interface. Assuming that the interface I is thin enough (*i.e.* that ℓ is small enough) let assume that the displacement $\boldsymbol{u}_I$ in I linearly bridges $\boldsymbol{u}_K|_{\partial K}$ to $\boldsymbol{u}_{\partial T}$ such that

$$\boldsymbol{u}_I(\boldsymbol{x}) = \frac{\boldsymbol{u}_{\partial T}(\mathbf{\Psi}^{-1}(\boldsymbol{x}_\ell)) - \boldsymbol{u}_K|_{\partial K}(\mathbf{\Psi}^{-1}(\boldsymbol{x}_o))}{\ell}x_0 + \boldsymbol{u}_K|_{\partial K}(\mathbf{\Psi}^{-1}(\boldsymbol{x}_o)) \tag{A.2}$$

where x_0 is the first coordinate of a point $\boldsymbol{x}$ in the local frame defined by $\mathbf{\Psi}$. The vector $\boldsymbol{x}_o$ denotes a point located in the plane $x_0 = 0$, and $\boldsymbol{x}_\ell$ a point on the plane $x_0 = \ell$, such that they share the same coordinates on their respective planes.

Displacement gradient in the interface. The derivative of $\boldsymbol{u}_I$ with respect to $\boldsymbol{X}$ yields

$$\frac{\partial u_{Ii}}{\partial X_j} = \sum_k \frac{\partial u_{Ii}}{\partial x_k}\frac{\partial x_k}{\partial X_j} = \frac{u_{\partial Ti}(\boldsymbol{\Psi}^{-1}(\boldsymbol{x}_\ell)) - u_{Ki}|_{\partial K}(\boldsymbol{\Psi}^{-1}(\boldsymbol{x}_o))}{\ell}Q_{0j} \tag{A.3}$$

which reads

$$\nabla\boldsymbol{u}_I(\boldsymbol{X}) = \frac{\boldsymbol{u}_{\partial T}(\boldsymbol{X}_\ell) - \boldsymbol{u}_K|_{\partial K}(\boldsymbol{X}_o)}{\ell} \otimes \boldsymbol{n} \tag{A.4}$$

where we have used the fact that the first row of the rotation matrix $\underset{\sim}{\boldsymbol{Q}}$ is given by $\boldsymbol{n}$. The points $\boldsymbol{X}_o$ and $\boldsymbol{X}_\ell$ are located on the normal plane to $\boldsymbol{n}$ on ∂K and ∂T respectively, in the reference frame.

Stress in the interface. As introduced in Section 3, the stress $\underset{\sim}{\boldsymbol{P}}_I$ is assumed constant along the direction $\boldsymbol{n}$ in I. By continuity of the traction force across ∂K, the following equality holds true

$$(\underset{\sim}{\boldsymbol{P}}_I - \underset{\sim}{\boldsymbol{P}}_K|_{\partial K}) \cdot \boldsymbol{n} = 0 \quad \text{in} \quad I \tag{A.5}$$

Internal Hu-Washizu in the interface. Let $L_{I,\text{int}}^{HW}$ the internal contribution of the Hu-Washizu Lagrangian in I

$$L_{I,\text{int}}^{HW} := \int_I \psi_I + (\nabla\boldsymbol{u}_I - \underset{\sim}{\boldsymbol{G}}_I) : \underset{\sim}{\boldsymbol{P}}_I \tag{A.6}$$

Let $C_I = \{v \in L^2(I) \mid v \cdot \boldsymbol{n} = \text{cste}\}$ the set of L^2-functions which are constant along the normal axis in I. For any function in C_I, the following equality holds true:

$$\int_I v\, dV = \int_{\partial K}\int_{\epsilon=0}^{\ell} v(1 - \alpha\epsilon)\, dS\, d\epsilon = \ell(1 - \frac{\alpha}{2}\ell)\int_{\partial K} v\, dS \tag{A.7}$$

Noticing that $\nabla\boldsymbol{u}_I \in C_I$, one has :

$$\begin{aligned}
\int_I \psi_I &= \ell(1 - \frac{\alpha}{2}\ell)\int_{\partial K}\frac{1}{2}\beta\frac{\ell}{h_T}\nabla\boldsymbol{u}_I : \nabla\boldsymbol{u}_I \\
&= \ell(1 - \frac{\alpha}{2}\ell)\int_{\partial K}\frac{\beta}{2\ell h_T}(\boldsymbol{u}_{\partial T} - \boldsymbol{u}_K|_{\partial K}) \otimes \boldsymbol{n} : (\boldsymbol{u}_{\partial T} - \boldsymbol{u}_K|_{\partial K}) \otimes \boldsymbol{n} \\
&= \ell(1 - \frac{\alpha}{2}\ell)\int_{\partial K}\frac{\beta}{2\ell h_T}\|\boldsymbol{u}_{\partial T} - \boldsymbol{u}_K|_{\partial K}\|^2 \\
&= (1 - \frac{\alpha}{2}\ell)\int_{\partial K}\frac{\beta}{2h_T}\|\boldsymbol{u}_{\partial T} - \boldsymbol{u}_K|_{\partial K}\|^2
\end{aligned} \tag{A.8}$$

Moreover, for $\underset{\sim}{\boldsymbol{P}}_I$ in C_I :

$$\begin{aligned}
\int_I \nabla\boldsymbol{u}_I : \underset{\sim}{\boldsymbol{P}}_I &= \ell(1 - \frac{\alpha}{2}\ell)\int_{\partial K}\nabla\boldsymbol{u}_I : \underset{\sim}{\boldsymbol{P}}_I \\
&= \ell(1 - \frac{\alpha}{2}\ell)\int_{\partial K}\frac{1}{\ell}(\boldsymbol{u}_{\partial T} - \boldsymbol{u}_K|_{\partial K}) \otimes \boldsymbol{n} : \underset{\sim}{\boldsymbol{P}}_I \\
&= (1 - \frac{\alpha}{2}\ell)\int_{\partial K}(\boldsymbol{u}_{\partial T} - \boldsymbol{u}_K|_{\partial K}) \cdot \underset{\sim}{\boldsymbol{P}}_K|_{\partial K} \cdot \boldsymbol{n}
\end{aligned} \tag{A.9}$$

where we have used (A.5). And Finally :

$$L_{I,\text{int}}^{HW} = (1 - \frac{\alpha}{2}\ell)\int_{\partial K}\frac{\beta}{2h_T}\|\boldsymbol{u}_{\partial T} - \boldsymbol{u}_K|_{\partial K}\|^2 + (1 - \frac{\alpha}{2}\ell)\int_{\partial K}(\boldsymbol{u}_{\partial T} - \boldsymbol{u}_K|_{\partial K}) \cdot \underset{\sim}{\boldsymbol{P}}_K|_{\partial K} \cdot \boldsymbol{n} - \int_I \underset{\sim}{\boldsymbol{G}}_I : \underset{\sim}{\boldsymbol{P}}_I \tag{A.10}$$

Total Hu-Washizu Lagrangian in the composite element. Injecting (A.6) in (11) yields

$$
L_T^{HW} = \int_K \psi_\Omega + (\nabla \boldsymbol{u}_K - \boldsymbol{G}_K) : \boldsymbol{P}_K + (1 - \frac{\alpha}{2}\ell) \int_{\partial K} (\boldsymbol{u}_{\partial T} - \boldsymbol{u}_K|_{\partial K}) \cdot \boldsymbol{P}_K|_{\partial K} \cdot \boldsymbol{n}
$$
$$
+ (1 - \frac{\alpha}{2}\ell) \int_{\partial K} \frac{\beta}{2h_T} \|\boldsymbol{u}_{\partial T} - \boldsymbol{u}_K|_{\partial K}\|^2 - \int_I \boldsymbol{G}_I : \boldsymbol{P}_I - \int_K \boldsymbol{f}_V \cdot \boldsymbol{u}_K - \int_I \boldsymbol{f}_V \cdot \boldsymbol{u}_I - \int_{\partial_N T} \boldsymbol{t}_{\partial_N T} \cdot \boldsymbol{u}_{\partial T}
$$

(A.11)

Since ℓ is arbitrary, let $\ell \to 0$, the interface region vanishes such that $I \to \emptyset$, $K \to T$ and $\partial K \to \partial T$, and the expression of the Hu–Washizu functional over the region T writes

$$
L_T^{HW} = \int_T \psi_\Omega + (\nabla \boldsymbol{u}_T - \boldsymbol{G}_T) : \boldsymbol{P}_T + \int_{\partial T} (\boldsymbol{u}_{\partial T} - \boldsymbol{u}_T|_{\partial T}) \cdot \boldsymbol{P}_T|_{\partial T} \cdot \boldsymbol{n} + \int_{\partial T} \frac{\beta}{2h_T} \|\boldsymbol{u}_{\partial T} - \boldsymbol{u}_T|_{\partial T}\|^2
$$
$$
- \int_T \boldsymbol{f}_V \cdot \boldsymbol{u}_T - \int_{\partial_N T} \boldsymbol{t}_{\partial_N T} \cdot \boldsymbol{u}_{\partial T}
$$

(A.12)

which concludes the development of equation (14).

Appendix A.2. Reconstructed gradient and Elliptic projection

This section aims at generalizing the elliptic projection property of the reconstructed gradient, as introduced in [29]. In the following, subspaces for the cell and faces approximations are not assumed to be polynomial necessarily.

Let $U(T)$ the space of cell kinematically admissible displacements, and $V(\partial T)$ that of face kinematically admissible displacements. The space for statically admissible stress and strain is denoted $S(T)$.

Let $U^h(T) \subset U(T)$ and $U^\perp(T) \subset U(T)$ such that $U(T) = U^h(T) \oplus U^\perp(T)$, and set $\boldsymbol{u}_T = \boldsymbol{u}_T^h + \boldsymbol{u}_T^\perp$ with $\boldsymbol{u}_T^h \in U^h(T)$ and $\boldsymbol{u}_T^\perp \in U^\perp(T)$ the orthogonal projections of $\boldsymbol{u}_T$ onto $U^h(T)$ and $U^\perp(T)$ respectively. Let $V^h(\partial T) \subset V(\partial T)$ and $\boldsymbol{u}_{\partial T}^h \in V^h(\partial T)$ the orthogonal projection of $\boldsymbol{u}_T$ onto $V^h(\partial T)$. The orthogonal projection of $\boldsymbol{u}_T$ onto $U^h(\bar{T}) = U^h(T) \times V^h(\partial T)$ is then the displacement pair $(\boldsymbol{u}_T^h, \boldsymbol{u}_{\partial T}^h)$. Let $S^h(T) = \{\boldsymbol{\tau}_T^h \in S(T) \mid \nabla \cdot \boldsymbol{\tau}_T^h \in U^h(T) \mid \boldsymbol{\tau}_T^h|_{\partial T} \cdot \boldsymbol{n} \in V^h(\partial T)\}$, and $\boldsymbol{G}_T^h \in S^h(T)$ the solution of (16) for $(\boldsymbol{u}_T^h, \boldsymbol{u}_{\partial T}^h)$ such that

$$
\int_T \boldsymbol{G}_T^h(\boldsymbol{u}_T^h, \boldsymbol{u}_{\partial T}^h) : \boldsymbol{\tau}_T^h = \int_T \nabla \boldsymbol{u}_T^h : \boldsymbol{\tau}_T^h + \int_{\partial T} (\boldsymbol{u}_{\partial T}^h - \boldsymbol{u}_T^h|_{\partial T}) \cdot \boldsymbol{\tau}_T^h|_{\partial T} \cdot \boldsymbol{n} \qquad \forall \boldsymbol{\tau}_T^h \in S^h(T)
$$

(A.13)

using the fact that $\boldsymbol{u}_{\partial T}^h$ is the projection of $\boldsymbol{u}_T$ onto $V^h(\partial T)$ and that $\boldsymbol{\tau}|_{\partial T} \cdot \boldsymbol{n} \in V^h(\partial T)$:

$$
\int_T \boldsymbol{G}_T^h(\boldsymbol{u}_T^h, \boldsymbol{u}_{\partial T}^h) : \boldsymbol{\tau}_T^h = \int_T \nabla \boldsymbol{u}_T^h : \boldsymbol{\tau}_T^h + \int_{\partial T} (\boldsymbol{u}_T|_{\partial T} - \boldsymbol{u}_T^h|_{\partial T}) \cdot \boldsymbol{\tau}_T^h|_{\partial T} \cdot \boldsymbol{n} \qquad \forall \boldsymbol{\tau}_T^h \in S^h(T)
$$
$$
= \int_T \nabla \boldsymbol{u}_T^h : \boldsymbol{\tau}_T^h + \int_{\partial T} \boldsymbol{u}_T^\perp|_{\partial T} \cdot \boldsymbol{\tau}_T^h|_{\partial T} \cdot \boldsymbol{n} \qquad \forall \boldsymbol{\tau}_T^h \in S^h(T)
$$

(A.14)

using the divergence theorem and the fact that $\nabla \cdot \boldsymbol{\tau}_T^h \in U^h(T)$, one has :

$$
\int_T \nabla \boldsymbol{u}_T^\perp : \boldsymbol{\tau}_T^h = \int_{\partial T} \boldsymbol{u}_T^\perp|_{\partial T} \cdot \boldsymbol{\tau}_T^h|_{\partial T} \cdot \boldsymbol{n}
$$

(A.15)

such that :

$$
\int_T \boldsymbol{G}_T^h(\boldsymbol{u}_T^h, \boldsymbol{u}_{\partial T}^h) : \boldsymbol{\tau}_T^h = \int_T \nabla \boldsymbol{u}_T^h : \boldsymbol{\tau}_T^h + \int_T \nabla \boldsymbol{u}_T^\perp : \boldsymbol{\tau}_T^h \qquad \forall \boldsymbol{\tau}_T^h \in S^h(T)
$$
$$
= \int_T \nabla \boldsymbol{u}_T : \boldsymbol{\tau}_T^h \qquad \forall \boldsymbol{\tau}_T^h \in S^h(T)
$$

(A.16)

which states that $\boldsymbol{G}_T^h(\boldsymbol{u}_T^h, \boldsymbol{u}_{\partial T}^h)$ is the orthogonal projection of $\nabla \boldsymbol{u}_T$ onto $S^h(T)$. By linearity of the algebraic trace operator, one has that $\text{Tr}(\boldsymbol{G}_T^h(\boldsymbol{u}_T^h, \boldsymbol{u}_{\partial T}^h))$ is the orthogonal projection of $\nabla \cdot \boldsymbol{u}$, which proves robustness of the method for linear elastic materials, since the Lamé coefficient λ acts on $\nabla \cdot \boldsymbol{u}$.

Appendix A.3. Operators in the axi-symmetric framework

This part specifies the formulation of HHO operators in the axi-symmetric framework.

Reconstructed gradient. For any displacement pair $(v_T^l, v_{\partial T}^k) \in U^h(T) \times V^h(\partial T)$, the component $G_{T\theta\theta}(v_{Tr}, v_{\partial Tr})$ solves

$$\int_T 2\pi r G_{T\theta\theta}(v_{Tr}, v_{\partial Tr})\tau_{T\theta\theta} = \int_T 2\pi r \frac{u_{Tr}}{r}\tau_{T\theta\theta} = \int_T 2\pi u_{Tr}\tau_{T\theta\theta} \quad \forall \underline{\tau}_T \in S(T) \tag{A.17}$$

In the radial and ordonal directions, *i.e.* $\forall i, j \in \{r, z\}$, the expression given in (16) is retrieved, and the component $G_{Tij}(v_{Ti}, v_{\partial Ti})$ solves

$$\int_T 2\pi r G_{Tij}(v_{Ti}, v_{\partial Ti})\tau_{Tij} = \int_T 2\pi r \frac{\partial u_{Ti}}{\partial j}\tau_{ij} - \int_{\partial T} 2\pi r(u_{\partial Ti} - u_{Ti}|_{\partial T})\tau_{Tij}|_{\partial T} n_j \quad \forall \underline{\tau}_T \in S(T) \tag{A.18}$$

Reconstructed higher order displacement. For any $\boldsymbol{d}_T^{k+1} \in D^h(T)$, the radial component w_{Tr}^{k+1} solves

$$\begin{aligned}
\int_T 2\pi r \Big(\sum_{i\in\{r,z\}} \frac{\partial w_{Tr}^{k+1}}{\partial i} \frac{\partial d_{Tr}^{k+1}}{\partial i} + \frac{w_{Tr}^{k+1}}{r} \frac{d_{Tr}^{k+1}}{r} \Big) &= \int_T 2\pi r \Big(\sum_{i\in\{r,z\}} \frac{\partial u_{Tr}}{\partial i} \frac{\partial d_{Tr}^{k+1}}{\partial i} + \frac{u_{Tr}}{r} \frac{d_{Tr}^{k+1}}{r} \Big) \\
&\quad + \int_{\partial T} 2\pi r \sum_{i\in\{r,z\}} (u_{\partial Tr} - u_{Tr}|_{\partial T}) \frac{\partial d_{Tr}^{k+1}}{\partial i}\Big|_{\partial T} n_i
\end{aligned} \tag{A.19}$$

where the mean value condition is not needed on the radial component of the higher order displacement since the left hand side of the system described by (A.19) depends directly on the displacement unknown and not only on its gradient as in (A.20). The ordinate component w_{Tz}^{k+1} solves :

$$\int_T 2\pi r \sum_{i\in\{r,z\}} \frac{\partial w_{Tz}^{k+1}}{\partial i} \frac{\partial d_{Tz}^{k+1}}{\partial i} = \int_T 2\pi r \sum_{i\in\{r,z\}} \frac{\partial u_{Tz}}{\partial i} \frac{\partial d_{Tz}^{k+1}}{\partial i} - \int_{\partial T} 2\pi r \sum_{i\in\{r,z\}} (u_{\partial Tz} - u_{Tz}|_{\partial T}) \frac{\partial d_{Tz}^{k+1}}{\partial i}\Big|_{\partial T} n_i \tag{A.20a}$$

$$\int_T 2\pi r w_{Tz}^{k+1} = \int_T 2\pi r u_{Tz} \tag{A.20b}$$

References

[1] W. Reed, T. Hill, Triangular mesh methods for the neutron transport equation, Tech. rep., United States, lA-UR–73-479 INIS Reference Number: 4080130 (1973).

[2] I. Babuska, The Finite Element Method with Penalty, Mathematics of Computation 27 (122) (1973) 221. doi:10.2307/2005611.
URL https://www.jstor.org/stable/2005611?origin=crossref

[3] V. J. Nitsche, Uber ein Yariationsprinzip zur Liisung von Dirichlet-Problemen bei Verwendung yon Teilr¨iumen, die keinen Randbedingungen unterworfen sind (1970) 7.

[4] P. Hansbo, M. G. Larson, Discontinuous Galerkin methods for incompressible and nearly incompressible elasticity by Nitsche's method, Computer Methods in Applied Mechanics and Engineering 191 (17-18) (2002) 1895–1908. doi:10.1016/S0045-7825(01)00358-9.
URL https://linkinghub.elsevier.com/retrieve/pii/S0045782501003589

[5] M. F. Wheeler, An Elliptic Collocation-Finite Element Method with Interior Penalties, SIAM Journal on Numerical Analysis 15 (1) (1978) 152–161. doi:10.1137/0715010.
URL http://epubs.siam.org/doi/10.1137/0715010

[6] B. Rivière, M. F. Wheeler, Optimal Error Estimates for Discontinuous Galerkin Methods Applied to Linear Elasticity Problems, Comput. Math. Appl 46 (2000) 141–163.

[7] A. Lew, P. Neff, D. Sulsky, M. Ortiz, Optimal BV estimates for a discontinuous Galerkin method for linear elasticity, Applied Mathematics Research eXpress 2004 (3) (2004) 73. doi:10.1155/S1687120004020052.
URL https://academic.oup.com/amrx/article-lookup/doi/10.1155/S1687120004020052

[8] F. Celiker, B. Cockburn, H. K. Stolarski, Locking-Free Optimal Discontinuous Galerkin Methods for Timoshenko Beams, SIAM Journal on Numerical Analysis 44 (6) (2006) 2297–2325.
URL http://www.jstor.org/stable/40232896

[9] S. C. Brenner, L.-y. Sung, Balancing domain decomposition for nonconforming plate elements, Numerische Mathematik 83 (1) (1999) 25–52. doi:10.1007/s002110050438.
URL https://doi.org/10.1007/s002110050438

[10] G. Engel, K. Garikipati, T. Hughes, M. Larson, L. Mazzei, R. Taylor, Continuous/discontinuous finite element approximations of fourth-order elliptic problems in structural and continuum mechanics with applications to thin beams and plates, and strain gradient elasticity, Computer Methods in Applied Mechanics and Engineering 191 (34) (2002) 3669–3750. doi:10.1016/S0045-7825(02)00286-4.
URL https://linkinghub.elsevier.com/retrieve/pii/S0045782502002864

[11] D. N. Arnold, F. Brezzi, L. D. Marini, A Family of Discontinuous Galerkin Finite Elements for the Reissner–Mindlin Plate, Journal of Scientific Computing 22 (1) (2005) 25–45. doi:10.1007/s10915-004-4134-8.
URL https://doi.org/10.1007/s10915-004-4134-8

[12] A. Ten Eyck, A. Lew, Discontinuous Galerkin methods for non-linear elasticity, International Journal for Numerical Methods in Engineering 67 (9) (2006) 1204–1243. doi:10.1002/nme.1667.
URL https://onlinelibrary.wiley.com/doi/10.1002/nme.1667

[13] L. Noels, R. Radovitzky, A general discontinuous Galerkin method for finite hyperelasticity. Formulation and numerical applications, International Journal for Numerical Methods in Engineering 68 (1) (2006) 64–97. doi:10.1002/nme.1699.
URL https://onlinelibrary.wiley.com/doi/10.1002/nme.1699

[14] C. Ortner, E. Süli, Discontinuous Galerkin Finite Element Approximation of Nonlinear Second-Order Elliptic and Hyperbolic Systems, SIAM Journal on Numerical Analysis 45 (4) (2007) 1370–1397, publisher: Society for Industrial and Applied Mathematics. doi:10.1137/06067119X.
URL https://epubs.siam.org/doi/10.1137/06067119X

[15] K. Shahbazi, P. F. Fischer, C. R. Ethier, A high-order discontinuous Galerkin method for the unsteady incompressible Navier–Stokes equations, Journal of Computational Physics 222 (1) (2007) 391–407. doi:10.1016/j.jcp.2006.07.029.
URL https://linkinghub.elsevier.com/retrieve/pii/S0021999106003585

[16] P.-O. Persson, J. Bonet, J. Peraire, Discontinuous Galerkin solution of the Navier–Stokes equations on deformable domains, Computer Methods in Applied Mechanics and Engineering 198 (17-20) (2009) 1585–1595. doi:10.1016/j.cma.2009.01.012.
URL https://linkinghub.elsevier.com/retrieve/pii/S0045782509000450

[17] R. Gracie, H. Wang, T. Belytschko, Blending in the extended finite element method by discontinuous Galerkin and assumed strain methods, International Journal for Numerical Methods in Engineering 74 (11) (2008) 1645–1669, _eprint: https://onlinelibrary.wiley.com/doi/pdf/10.1002/nme.2217. doi:10.1002/nme.2217.
URL https://onlinelibrary.wiley.com/doi/abs/10.1002/nme.2217

[18] Y. Shen, A. Lew, Stability and convergence proofs for a discontinuous-Galerkin-based extended finite element method for fracture mechanics, Computer Methods in Applied Mechanics and Engineering 199 (37) (2010) 2360–2382. doi:10.1016/j.cma.2010.03.008.
URL https://www.sciencedirect.com/science/article/pii/S0045782510000848

[19] J. K. Djoko, F. Ebobisse, A. T. McBride, B. D. Reddy, A discontinuous Galerkin formulation for classical and gradient plasticity – Part 1: Formulation and analysis, Computer Methods in Applied Mechanics and Engineering 196 (37) (2007) 3881–3897. doi:10.1016/j.cma.2006.10.045.
URL https://www.sciencedirect.com/science/article/pii/S0045782507001144

[20] J. K. Djoko, F. Ebobisse, A. T. McBride, B. D. Reddy, A discontinuous Galerkin formulation for classical and gradient plasticity. Part 2: Algorithms and numerical analysis, Computer Methods in Applied Mechanics and Engineering 197 (1) (2007) 1–21. doi:10.1016/j.cma.2007.06.027.
URL https://www.sciencedirect.com/science/article/pii/S0045782507002964

[21] B. Cockburn, J. Gopalakrishnan, R. Lazarov, Unified Hybridization of Discontinuous Galerkin, Mixed, and Continuous Galerkin Methods for Second Order Elliptic Problems, SIAM Journal on Numerical Analysis 47 (2) (2009) 1319–1365. doi:10.1137/070706616.
URL http://epubs.siam.org/doi/10.1137/070706616

[22] S.-C. Soon, B. Cockburn, H. K. Stolarski, A hybridizable discontinuous Galerkin method for linear elasticity: AN HDG METHOD, International Journal for Numerical Methods in Engineering 80 (8) (2009) 1058–1092. doi:10.1002/nme.2646.
URL https://onlinelibrary.wiley.com/doi/10.1002/nme.2646

[23] S.-C. Soon, Hybridizable discontinuous Galerkin method for solid mechanics, Ph.D. thesis, University of Minnesota (2008).

[24] N. Nguyen, J. Peraire, B. Cockburn, An implicit high-order hybridizable discontinuous Galerkin method for linear convection–diffusion equations, Journal of Computational Physics 228 (9) (2009) 3232–3254. doi:10.1016/j.jcp.2009.01.030.
URL https://linkinghub.elsevier.com/retrieve/pii/S0021999109000308

[25] N. Nguyen, J. Peraire, B. Cockburn, An implicit high-order hybridizable discontinuous Galerkin method for nonlinear convection–diffusion equations, Journal of Computational Physics 228 (23) (2009) 8841–8855. doi:10.1016/j.jcp.2009.08.030.
URL https://linkinghub.elsevier.com/retrieve/pii/S0021999109004756

[26] N. Nguyen, J. Peraire, B. Cockburn, A hybridizable discontinuous Galerkin method for Stokes flow, Computer Methods in Applied Mechanics and Engineering 199 (9-12) (2010) 582–597. doi:10.1016/j.cma.2009.10.007.
URL https://linkinghub.elsevier.com/retrieve/pii/S0045782509003521

[27] N. Nguyen, J. Peraire, B. Cockburn, An implicit high-order hybridizable discontinuous Galerkin method for the incompressible Navier–Stokes equations, Journal of Computational Physics 230 (4) (2011) 1147–1170. doi:10.1016/j.jcp.2010.10.032.
URL https://linkinghub.elsevier.com/retrieve/pii/S0021999110005887

[28] N. Nguyen, J. Peraire, Hybridizable discontinuous Galerkin methods for partial differential equations in continuum mechanics, Journal of Computational Physics 231 (18) (2012) 5955–5988. doi:10.1016/j.jcp.2012.02.033.
URL https://linkinghub.elsevier.com/retrieve/pii/S0021999112001544

[29] D. A. Di Pietro, A. Ern, A hybrid high-order locking-free method for linear elasticity on general meshes, Computer Methods in Applied Mechanics and Engineering 283 (2015) 1–21. doi:10.1016/j.cma.2014.09.009.
URL https://linkinghub.elsevier.com/retrieve/pii/S0045782514003181

[30] D. A. Di Pietro, A. Ern, S. Lemaire, An Arbitrary-Order and Compact-Stencil Discretization of Diffusion on General Meshes Based on Local Reconstruction Operators, Computational Methods in Applied Mathematics 14 (4) (2014) 461–472. doi:10.1515/cmam-2014-0018.

URL `https://www.degruyter.com/document/doi/10.1515/cmam-2014-0018/html`
[31] D. A. Di Pietro, A. Ern, A. Linke, F. Schieweck, A discontinuous skeletal method for the viscosity-dependent Stokes problem, Computer Methods in Applied Mechanics and Engineering 306 (2016) 175–195. `doi:10.1016/j.cma.2016.03.033`.
URL `https://linkinghub.elsevier.com/retrieve/pii/S0045782516301189`
[32] D. A. Di Pietro, S. Krell, A Hybrid High-Order Method for the Steady Incompressible Navier–Stokes Problem, Journal of Scientific Computing 74 (3) (2018) 1677–1705. `doi:10.1007/s10915-017-0512-x`.
URL `http://link.springer.com/10.1007/s10915-017-0512-x`
[33] D. Boffi, M. Botti, D. A. Di Pietro, A Nonconforming High-Order Method for the Biot Problem on General Meshes, SIAM Journal on Scientific Computing 38 (3) (2016) A1508–A1537. `doi:10.1137/15M1025505`.
URL `http://epubs.siam.org/doi/10.1137/15M1025505`
[34] M. Botti, D. A. Di Pietro, P. Sochala, A Hybrid High-Order Method for Nonlinear Elasticity, SIAM Journal on Numerical Analysis 55 (6) (2017) 2687–2717. `doi:10.1137/16M1105943`.
URL `https://epubs.siam.org/doi/10.1137/16M1105943`
[35] T. Belytschko, Nonlinear Finite Elements for Continua and Structures 834.
[36] K. Washizu, Variational methods in elasticity and plasticity, 2nd Edition, International series of monographs in aeronautics and astronautics. Division I: solid and structural mechanics, v. 9, Pergamon Press, Oxford, New York, 1974.
[37] D. Al Akhrass, J. Bruchon, S. Drapier, S. Fayolle, Integrating a logarithmic-strain based hyperelastic formulation into a three-field mixed finite element formulation to deal with incompressibility in finite-strain elastoplasticity, Finite Elements in Analysis and Design 86 (2014) 61–70. `doi:10.1016/j.finel.2014.04.004`.
URL `https://linkinghub.elsevier.com/retrieve/pii/S0168874X14000596`
[38] J. C. Simo, R. L. Taylor, Quasi-incompressible finite elasticity in principal stretches. continuum basis and numerical algorithms, Computer Methods in Applied Mechanics and Engineering 85 (3) (1991) 273–310. `doi:10.1016/0045-7825(91)90100-K`.
URL `https://linkinghub.elsevier.com/retrieve/pii/004578259190100K`
[39] J. Simo, R. Taylor, K. Pister, Variational and projection methods for the volume constraint in finite deformation elasto-plasticity, Computer Methods in Applied Mechanics and Engineering 51 (1-3) (1985) 177–208. `doi:10.1016/0045-7825(85)90033-7`.
URL `https://linkinghub.elsevier.com/retrieve/pii/0045782585900337`
[40] J. C. Simo, T. J. R. Hughes, On the Variational Foundations of Assumed Strain Methods, Journal of Applied Mechanics 53 (1) (1986) 51–54. `doi:10.1115/1.3171737`.
URL `https://asmedigitalcollection.asme.org/appliedmechanics/article/53/1/51/390714/On-the-Variational-Foundations-of-Assumed-Strain`
[41] J. C. Simo, M. S. Rifai, A class of mixed assumed strain methods and the method of incompatible modes, International Journal for Numerical Methods in Engineering 29 (8) (1990) 1595–1638. `doi:10.1002/nme.1620290802`.
URL `https://onlinelibrary.wiley.com/doi/10.1002/nme.1620290802`
[42] D. A. Di Pietro, J. Droniou, A. Ern, A Discontinuous-Skeletal Method for Advection-Diffusion-Reaction on General Meshes, SIAM Journal on Numerical Analysis 53 (5) (2015) 2135–2157. `doi:10.1137/140993971`.
URL `http://epubs.siam.org/doi/10.1137/140993971`
[43] B. Cockburn, J. Shen, An algorithm for stabilizing hybridizable discontinuous Galerkin methods for nonlinear elasticity, Results in Applied Mathematics 1 (2019) 100001. `doi:10.1016/j.rinam.2019.01.001`.
URL `https://linkinghub.elsevier.com/retrieve/pii/S2590037419300019`
[44] M. Abbas, A. Ern, N. Pignet, A Hybrid High-Order method for incremental associative plasticity with small deformations, Computer Methods in Applied Mechanics and Engineering 346 (2019) 891–912. `doi:10.1016/j.cma.2018.08.037`.
URL `https://linkinghub.elsevier.com/retrieve/pii/S0045782518304353`
[45] M. Abbas, A. Ern, N. Pignet, Hybrid High-Order methods for finite deformations of hyperelastic materials, Computational Mechanics 62 (4) (2018) 909–928. `doi:10.1007/s00466-018-1538-0`.
URL `http://link.springer.com/10.1007/s00466-018-1538-0`
[46] B. Schröder, D. Kuhl, Small strain plasticity: classical versus multifield formulation, Archive of Applied Mechanics 85 (8) (2015) 1127–1145. `doi:10.1007/s00419-015-0984-9`.
URL `http://link.springer.com/10.1007/s00419-015-0984-9`
[47] C. Miehe, N. Apel, M. Lambrecht, Anisotropic additive plasticity in the logarithmic strain space: modular kinematic formulation and implementation based on incremental minimization principles for standard materials, Computer Methods in Applied Mechanics and Engineering 191 (47-48) (2002) 5383–5425. `doi:10.1016/S0045-7825(02)00438-3`.
URL `https://linkinghub.elsevier.com/retrieve/pii/S0045782502004383`